Geosci. Model Dev. Discuss., https://doi.org/10.5194/gmd-2018-105
Manuscript under review for journal Geosci. Model Dev.
Discussion started: 2 May 2018


Geoscientific Model Development Discussions

# The GRISLI ice sheet model (version 2.0): calibration and validation for multi-millennial changes of the Antarctic ice sheet

Aurélien Quiquet[1], Christophe Dumas[1], Catherine Ritz[2], Vincent Peyaud[2], and Didier M. Roche[1,3]

[1]Laboratoire des Sciences du Climat et de l'Environnement (LSCE), UMR8212, CEA/CNRS-INSU/UVSQ, Gif-sur-Yvette Cedex, France
[2]Université Grenoble Alpes, CNRS, IRD, IGE, F-38000 Grenoble, France
[3]Earth and Climate Cluster, Faculty of Science, Vrije Universiteit Amsterdam, Amsterdam, the Netherlands

*Correspondence to:* A. Quiquet (aurelien.quiquet@lsce.ipsl.fr)

**Abstract.**

In this paper we present the GRISLI (Grenoble Ice Sheet and Land Ice) model in its newest revision (version 2.0). Whilst GRISLI is applicable to any given geometry, we focus here on the Antarctic ice sheet because it highlights the importance of grounding line dynamics. Important improvements have been implemented since its original version (Ritz et al., 2001) including notably an explicit flux computation at the grounding line based on the analytical formulations of Schoof (2007) and Tsai et al. (2015) and a basal hydrology model. A calibration of the mechanical parameters of the model based on an ensemble of 150 members sampled with a Latin Hypercube method is used. The ensemble members performance is assessed relative to the deviation from present-day observed Antarctic ice thickness. The model being designed for multi-millenial long-term integrations, we also present glacial-interglacial ice sheet changes throughout the last 400 kyr using the best ensemble members. To achieve this goal, we construct a simple climatic perturbation of present-day climate forcing fields based on two climate proxies, both atmospheric and oceanic. The model is able to reproduce expected grounding line advances during glacials and subsequent retreats during terminations with reasonable glacial-interglacial ice volume changes.

## 1 Introduction

Continental ice sheets are a major component for the Earth system dynamics on a variety of timescales through multiple feedbacks such as surface albedo, gravity waves and freshwater flux to the ocean. Over the last decades, modern observation techniques of the Greenland and Antarctic ice sheets (e.g. altimetry, gravimetry, echo sounding) have shown important changes such as an increase in surface and sub-shelf melt, glacier speed-up, dynamical thinning and drastic calving events (e.g. Mouginot et al., 2015; Paolo et al., 2015; Hall et al., 2013; Pritchard et al., 2009). Whilst the contribution of these ice sheets to global sea level in the future is largely uncertain, there are evidences of sea level rise as fast as four metres per century in the past (e.g. Fairbanks, 1989; Hanebuth et al., 2000; Deschamps et al., 2012). The study of well-recorded past events can help us to constrain the fate of the ice sheets in a warming Earth and to disentangle the role of the different processes leading to rapid ice sheet destabilisation. The surface elevation feedback on ice sheet surface mass balance has often been proposed as a major driver for rapid northern Hemisphere ice sheets disintegration (e.g. Abe-Ouchi et al., 2013; Gregoire et al., 2012). An other

Geosci. Model Dev. Discuss., https://doi.org/10.5194/gmd-2018-105
Manuscript under review for journal Geosci. Model Dev.
Discussion started: 2 May 2018




source of instability, for marine ice sheets such as the palaeo Kara-Barents or present-day Antarctic ice sheets, is related to the fact that the bedrock presents a retrograde slope from the grounding line and deepens well below sea level due, for instance, to isostatic adjustment or within glacial troughs. Such properties lead to the marine ice sheet instability (MISI, Weertman, 1974; Schoof, 2007) responsible for a fast and irreversible retreat of the grounding line in response to an initial perturbation such as local sea level change and/or increase in basal melting rate below ice shelves. Such processes are expected to play a crucial role for the stability of the Antarctic ice sheet in the future (e.g. Favier et al., 2014). Additional instabilities may also occur on prograde bed slopes and have been attributed to cliff instabilities and the associated decrease in ice-shelf buttressing (marine ice cliff instability, MICI, Pollard et al., 2015).

Because of the variety in temporal and spatial scales but also due to the lack of crucial observations (e.g. basal conditions and internal thermo-mechanics), continental ice sheets are difficult to model. Most numerical models consider ice sheets as an incompressible fluid, where motion can be described with the Navier-Stokes equations. Even if some processes have generally to be parameterised (e.g. ice anisotropy), the complete set of equations can be solved explicitly and does not require the use of any approximation. State of the art continental ice sheet models, namely the Full-Stokes models, solve explicitly all the terms in the stress tensor (Gillet-Chaulet et al., 2012; Larour et al., 2012). Recent applications are promising but, due to computational cost, continental scale applications are currently limited to a few centuries. As such, they are not yet the right tool for palaeo-reconstructions or multi-millenial future projections.

Conversely, in order to decrease the degree of complexity, simpler models were historically developed that make use of the small aspect ratio of ice sheets (vertical to horizontal scale ratio) to derive approximations for the Navier-Stokes equations (Hindmarsh, 2004). Such models present the advantage to be much cheaper compared to Full-Stokes models, allowing for multi-millenial integrations. They are well-suited to study slow feedbacks such as glacio-isostasy or the impact of temperature and surface mass balance perturbations diffusion. The Grenoble ice sheet and land ice (GRISLI) model belongs to the latter category (Ritz et al., 2001). GRISLI consists of the combination of the inland ice model of Ritz (1992) & Ritz et al. (1997) and the ice shelf model of Rommelaere and Ritz (1996), extended to the case of ice streams treated as *dragging ice shelves*, GRISLI being at that time the first large scale ice sheet model with an hybrid shallow ice / shallow shelf system of equations. Whilst since Ritz et al. (2001) the fundamental equations for ice dynamics have not drastically changed, the model has nonetheless benefited from the numerous works which used it. To date, 30 papers published or in peer-review discuss GRISLI model simulation results. The range of applications have been very wide ranging from ice sheet reconstructions for deep-time palaeo-climate (e.g. Benn et al., 2015; Donnadieu et al., 2011; Ladant et al., 2014) and Quaternary (e.g. Peyaud et al., 2007; Alvarez-Solas et al., 2013; Quiquet et al., 2013; Colleoni et al., 2016) to future sea level rise projections (e.g. Ritz et al., 2015; Peano et al., 2017). GRISLI has participated in several inter-comparison exercises (Calov et al., 2010; Edwards et al., 2014; Koenig et al., 2015; Goelzer et al., 2017) and has been coupled to climate models of various complexities (e.g. Philippon et al., 2006; Roche et al., 2014; Le clec'h et al., 2018).

Geosci. Model Dev. Discuss., https://doi.org/10.5194/gmd-2018-105
Manuscript under review for journal Geosci. Model Dev.
Discussion started: 2 May 2018


Geoscientific Model Development Discussions
Open Access
EGU

The aim of our current study is to provide a technical description of the GRISLI model in its current version (GRISLI version 2.0, hereafter GRISLI), including the several additional features from Ritz et al. (2001). In particular, we have now included an explicit flux computation at the grounding line following the analytical formulation from Schoof (2007) and Tsai et al. (2015) in order to have a better representation of the MISI. In addition, we present a simple calibration of the mechanical parameters suitable for multi-millenia integrations and we show an example of the model response to glacial-interglacial forcing.

In Sec. 2 we describe the fundamental equations of the GRISLI ice sheet model with a particular emphasis on the model developments departing from Ritz et al. (2001). In sec. 3, we present a simple calibration methodology which aims at reproducing the observed present-day Antarctic ice sheet geometry. In Sec. 4, we discuss the ability of the model to simulate the Antarctic ice sheet changes over the last four glacial-interglacial cycles.

## 2 The GRISLI ice sheet model

GRISLI constitutive equations were presented in Ritz et al. (2001) and we aim here at giving a broad comprehensive description of the current model version, with its latest functionalities. Major model parameters are listed in Tab. 1.

### 2.1 Ice thermo-mechanics

#### 2.1.1 Ice deformation and mass conservation

GRISLI considers the ice sheet as solely formed of pure ice with a constant and homogeneous density ($\rho_{ice}$). In this approximation, the ice being considered as an incompressible fluid, the mass conservation equation can be written as:

$$\nabla \mathbf{u} = \frac{\partial u_x}{\partial x} + \frac{\partial u_y}{\partial y} + \frac{\partial u_z}{\partial z} = 0 \tag{1}$$

with $(u_x, u_y, u_z)$ the Cartesian components of the ice velocity field.

The vertically integrated expression of the mass conservation equation provides the equation for the ice thickness, $H$:

$$\frac{\partial H}{\partial t} = -\frac{\partial H \bar{u_x}}{\partial x} - \frac{\partial H \bar{u_y}}{\partial y} + M - b_{melt} \tag{2}$$

with $\bar{u_x}$ and $\bar{u_y}$ the vertically integrated $x$ and $y$ velocities, $M$ the surface mass balance and $b_{melt}$ is the basal melting rate.

The quasi-static approximation is used for the velocity field, in which the inertial terms of the momentum conservation equation are ignored. The gravity force being the sole external force acting on an infinitesimal cube of ice, we have:

$$\begin{cases} \frac{\partial \sigma_x}{\partial x} + \frac{\partial \tau_{xy}}{\partial y} + \frac{\partial \tau_{xz}}{\partial z} = 0 \\ \frac{\partial \tau_{xy}}{\partial x} + \frac{\partial \sigma_y}{\partial y} + \frac{\partial \tau_{yz}}{\partial z} = 0 \\ \frac{\partial \tau_{xz}}{\partial x} + \frac{\partial \tau_{yz}}{\partial y} + \frac{\partial \sigma_z}{\partial z} = \rho_i g \end{cases} \tag{3}$$

Geosci. Model Dev. Discuss., https://doi.org/10.5194/gmd-2018-105
Manuscript under review for journal Geosci. Model Dev.
Discussion started: 2 May 2018




where $\sigma_{i=x,y,z}$, respectively $\tau_{ij=x,y,z}$, are the longitudinal, respectively shearing, stress tensor terms.

The pressure is defined as the first invariant of the stress tensor:

$$-P = \frac{\sigma_x + \sigma_y + \sigma_z}{3} \tag{4}$$

The deviatoric stress tensor is defined as (for $i, j = x, y, z$):

$$\tau'_{ij} = \tau_{ij} + \delta_{ij} P \tag{5}$$

with $\delta_{ij}$ being 1 for $i = j$, 0 otherwise.

Assuming isotropy, the deviatoric stress and the deformation rate $\dot{\epsilon_{ij}}$ are related by:

$$\tau'_{ij} = 2\eta\dot{\varepsilon_{ij}} \tag{6}$$

where $\eta$ is the ice viscosity.

Alike most ice sheet models, GRISLI considers the ice as a non-Newtonian viscous fluid following a Norton-Hoff constitutive law (commonly named Glen flow law):

$$\frac{1}{\eta} = B_{AT}\tau^{n-1} \tag{7}$$

where $B_{AT}$ is a temperature-dependent coefficient following an Arrhenius law, and $\tau$ is the effective shear stress, defined as:

$$\tau^2 = \frac{1}{2}\sum_{i,j}\tau_{ij}^2 \tag{8}$$

The Glen flow law is an empirical formulation, derived from laboratory experiments. However, laboratory experiments fail at reproducing the range of deviatoric stress values expected in real ice sheets. The timescale over which this stress is applied in real ice sheets is also not reproducible in laboratories. If most modelling studies agree to use $n = 3$ for the Glen flow law exponent, there is room for uncertainties as a few studies suggest the possibility for a smaller exponent for small stress regime (Duval and Lliboutry, 1985; Pimienta, 1987; Pettit and Waddington, 2003). One particularity of GRISLI is the possibility to simultaneously use a Glen viscosity with $n = 3$ and a linear, Newtonian, viscosity with $n = 1$ (Dumas, 2002). In this case, the two contributions simply add up:

$$2\,\dot{\varepsilon}_{ij} = \left(B_{AT1} + \tau^2 B_{AT3}\right)\,\tau'_{ij} \tag{9}$$

Alike other large scale ice sheet models, GRISLI does not take into account explicitly anisotropy. Anisotropy tends to facilitate deformation due to vertical shear (i.e. in the slow flowing regions, treated with the SIA), but reduces the deformation due to longitudinal stress (i.e. in the fast flowing regions, treated with the SSA regions). In GRISLI, a flow enhancement factor is applied in the Glen equation used in the SIA (Eq. 7) to favour longitudinal deformations. At the same time, a fixed ratio between the SIA and SSA enhancement factor is used, typically ranging from 5:1 to 10:1, as suggested by Ma et al. (2010).

Geosci. Model Dev. Discuss., https://doi.org/10.5194/gmd-2018-105
Manuscript under review for journal Geosci. Model Dev.
Discussion started: 2 May 2018


Geoscientific Model Development Discussions
Open Access
EGU

### 2.1.2 Ice velocity

The velocity in GRISLI is computed for the entire domain as the superposition of the shallow ice approximation (SIA) and the shallow shelf approximation (SSA) components.

The SIA (Hutter, 1982) assumes that the horizontal derivatives are much smaller than the vertical derivatives, which is generally true for the major part of the ice sheet where the gravity driven flow induces a slow motion of the ice. GRISLI uses the zero order of the SIA approximation in which the stress tensor components simplified to:

$$\begin{cases} \tau_{xz} = \rho_i g \frac{\partial S}{\partial x}(S-z) \\ \\ \tau_{yz} = \rho_i g \frac{\partial S}{\partial y}(S-z) \end{cases} \tag{10}$$

with $S$ the surface elevation. The vertical velocity profile computed as an integral from the bedrock (for $i = x, y, z$):

$$u_i(z) = u_{ib} + \int_B^z 2\,\dot{\varepsilon}_{iz}\,dz \tag{11}$$

where $u_{ib}$ is the $i$ component of the basal velocity.

The basal velocity can be computed with a sliding law (e.g. Bindschadler, 1983). However, recent versions of GRISLI use the shallow shelf approximation (SSA) as a sliding law as suggested by Bueler and Brown (2009). In this case, similarly to Winkelmann et al. (2011) we simply add up the two contributions of the SIA and SSA for the whole domain which ensure a smooth transition from non-sliding frozen regions to sliding over a thawed bed.

For the fast flowing regions the vertical stresses are much smaller than the longitudinal shear stresses. In this case, the velocity fields with the SSA (MacAyeal, 1989) reduced to the following elliptic equations:

$$\begin{cases} \frac{\partial}{\partial x}\left(2\bar{\eta}H\,(2\,\frac{\partial u_x}{\partial x}+\frac{\partial u_y}{\partial y})\right)+\frac{\partial}{\partial y}\left(\bar{\eta}H\,(\frac{\partial u_x}{\partial y}+\frac{\partial u_y}{\partial x})\right)=\rho g H\,\frac{\partial S}{\partial x}-\tau_{bx} \\ \\ \frac{\partial}{\partial y}\left(2\bar{\eta}H\,(2\,\frac{\partial u_y}{\partial y}+\frac{\partial u_x}{\partial x})\right)+\frac{\partial}{\partial x}\left(\bar{\eta}H\,(\frac{\partial u_y}{\partial x}+\frac{\partial u_x}{\partial y})\right)=\rho g H\,\frac{\partial S}{\partial y}-\tau_{by} \end{cases} \tag{12}$$

where $S$ is the surface topography and $\tau_b$ is the basal drag. The velocities $u_x$ and $u_y$ are identical along the vertical dimension.

The condition at the front of the ice shelf is given by the balance between the water pressure and the horizontal longitudinal stress (see also numerical feature)

### 2.1.3 Basal drag

For floating ice shelves, the basal drag, $\tau_b$, is zero. For cold-based grounded ice we impose a large enough basal drag (typically $10^5 Pa$) to ensure virtually no-slip conditions on the bedrock. For temperate-based grounded ice, a power-law basal friction

Geosci. Model Dev. Discuss., https://doi.org/10.5194/gmd-2018-105
Manuscript under review for journal Geosci. Model Dev.
Discussion started: 2 May 2018




(Weertman, 1957) is assumed:

$$\begin{cases} \tau_{bx}^{m} = -\beta\, u_{bx} \\ \\ \tau_{by}^{m} = -\beta\, u_{by} \end{cases} \tag{13}$$

where the basal drag coefficient $\beta$ is positive. In the experiment presented here, we assume the presence of a sediment at the base of the ice sheet allowing for a viscous deformation ($m = 1$).

In some recent applications of GRISLI, the basal drag coefficient has been inferred with an inverse method in order to match present-day ice sheet geometry (Ritz et al., 2015; Le clec'h et al., 2018). This approach has been followed to participate in the first phase of the recent ice sheet model intercomparison project (ISMIP6, Nowicki et al., 2016) for both the Greenland (Goelzer et al., 2017) and Antarctic ice sheets. In this context, GRISLI achieves to provide sea level rise projections by the end of the century in line with the results from more complex model (Edwards et al., 2014; Goelzer et al., 2017).

However, inverse methods do not provide information for grid points that are not glaciated today by construction. As such they are not applicable for palaeo reconstructions of the American or Eurasian ice sheets. More generally, inverse methods are no longer appropriate for long-term integrations, either palaeo or future, when ice thickness is very different from its present state and especially when ice boundary migrates from its present-day position. This motivates the use of a basal drag coefficient depending on GRISLI internal variables. We generally assume that its value is modulated by the effective water pressure, $N$, at the base of the ice sheet:

$$\beta = C_f N \tag{14}$$

with $C_f$ an internal parameter that needs calibration.

In our approach, any temperate-based grounded point will have a non-zero sliding velocity, depending on the $C_f$ factor used. Previous works have used additional criteria to limit the extension of these ice streams. For example, Alvarez-Solas et al. (2010) only compute Eq. 14 where the present-day sediment thickness exceeds a certain threshold whilst Quiquet et al. (2013) restrict this to large-scale valleys. However these approaches have flaws. For example, the sediment distribution is only poorly known below present-day ice sheets and its past evolution is largely uncertain. Also, the definition of a typical spatial scale for ice streams is somehow arbitrary. For these reasons, in the following we use the simplest approach and compute Eq. 14 for any temperate-based grid point.

#### 2.1.4 Flux at the grounding line

In Ritz et al. (2001) the position of the grounding line was computed from a simple floatation criterion with no additional flux correction. Such an approach is in theory only valid for a very high spatial resolution, within tenths of meters, at the vicinity of the grounding line (Durand et al., 2009). Because the model runs typically at a much coarser resolution, in GRISLI version

Geosci. Model Dev. Discuss., https://doi.org/10.5194/gmd-2018-105
Manuscript under review for journal Geosci. Model Dev.
Discussion started: 2 May 2018




2.0 we have implemented an explicit flux computation at the grounding line based on the analytical formulations from Schoof (2007) and Tsai et al. (2015). The two formulations differ from the assumption made on the sediment rheology.

The flux at the grounding line following Schoof (2007) is:

$$q_{gl}^{S} = -\left(\frac{\bar{A}(\rho_i g)^{n+1}(1-\rho_i/\rho_w)^n}{4^n \beta}\right)^{\frac{m}{m+1}} H_{gl}^{\frac{m(n+3)+1}{m+1}} \phi_{bf}^{\frac{m\ n}{m+1}} \tag{15}$$

with $n$ and $m$ being the exponents in the Glen flow law (Eq. 7) and in the friction law (Eq. 13) respectively, $\bar{A}$ the vertically integrated temperature dependent coefficient in the Glen flow law ($B_{AT}$, Eq. 7), $H_{gl}$ the ice thickness at the grounding line, and $\phi_{bf}$ a back force coefficient to take into account the buttressing role of ice shelves. $\beta$ is the basal drag coefficient presented in Eq. 13.

Conversely, Tsai et al. (2015) proposed:

$$q_{gl}^{T} = Q_0 \frac{8\bar{A}(\rho_i g)^n}{4^n f} (1-\rho_i/\rho_w)^{n-1} H_g^{n+2} \phi_{bf}^{n-1} \tag{16}$$

with $Q_0 = 0.61$. In this case, the basal drag is assumed to vanish at the grounding and as such the coefficient $\beta$ is not used. Instead Tsai et al. (2015) suggests a constant and homogeneous basal friction coefficient $f$ set to $0.6$.

In GRISLI, from the last grounded point in the direction of the flow, we compute the subgrid position of the grounding line in the $x$ and $y$ directions linearly interpolating the floatation criterion. From this position, the flux at the grounding line is calculated using Eq. 15 or Eq. 16. Then the value of the flux is linearly interpolated to the two closest downstream and upstream velocity grid points similarly to Fürst (2013).

To evaluate the back force coefficient $\phi_{bf}$, we solve the velocity equation twice, with and without ice shelves. The ratio in velocity for the grounded ice sheet points provides the back force coefficient $\phi_{bf}$. In the model, to inhibit the buttressing role of ice shelves without changes in geometry, they are assigned a very small viscosity so that they do not exert any back force. We acknowledge the fact that this approach is computationally expensive but it allows for more accurate estimate for the buttressing role of ice shelves in the model.

### 2.1.5 Calving

Ice front calving is not modelled explicitly. Instead, we used a simple ice thickness threshold criterion. Because this simple scheme can prevent ice shelf extension, we also maintain downstream ice shelf grid-points neighbouring the last grid-points meeting the criterion. The cut-off threshold may vary in space (e.g. oceanic depth dependency) and time. In the following, we use a constant and homogeneous thickness criterion (set to 250 m, roughly corresponding to the observed present-day Antarctic ice shelves front).

Geosci. Model Dev. Discuss., https://doi.org/10.5194/gmd-2018-105
Manuscript under review for journal Geosci. Model Dev.
Discussion started: 2 May 2018




### 2.1.6 Temperature coupling

Regarding the thermo-mechanical coupling, GRISLI solves the general advection-diffusion equation of temperature:

$$\frac{\partial T}{\partial t} = \underbrace{\frac{1}{\rho_i c}\frac{\partial}{\partial x}\left(k_i \frac{\partial T}{\partial x}\right) + \frac{1}{\rho_i c}\frac{\partial}{\partial y}\left(k_i \frac{\partial T}{\partial y}\right)}_{\text{horizontal diffusion}} \underbrace{+\frac{1}{\rho_i c}\frac{\partial}{\partial z}\left(k_i \frac{\partial T}{\partial z}\right)}_{\text{vertical diffusion}}$$
$$\underbrace{-u_x \frac{\partial T}{\partial x} - u_y \frac{\partial T}{\partial y}}_{\text{horizontal advection}} \underbrace{-u_z \frac{\partial T}{\partial z}}_{\text{vertical advection}} \underbrace{+\frac{Q}{\rho_i c}}_{\text{heat production}} \tag{17}$$

with $k_i$ the thermal conductivity of the ice and $c$ the heat capacity.

Horizontal diffusion is assumed to be much smaller than the vertical one and is therefore neglected.

The heat production is given by Hutter (1983) (for $i, j = x, y, z$):

$$Q = \sum_{i,j} \dot{\varepsilon}_{ij} \tau_{ij} \tag{18}$$

At the ice sheet surface, due to the absence of an explicit snowpack model, ice temperature is assumed to be equal to the near-surface air annual temperature (but not greater than zero). Depending on the surface mass balance parametrisation, the latent heat release due to refreezing is transferred to the first ice layer.

A geothermal heat flux $\phi_0$ is applied at the base of a 3 km thick bedrock layer with a Neumann boundary condition:

$$\phi_0 = -k_b \frac{\partial T}{\partial z}|_{bedrock} \tag{19}$$

with $k_b$ the bedrock thermal conductivity.

Similarly to what is done for ice temperature, the heat equation is solved in the bedrock with Eq. 17 but with no advection nor heat production. From the temperature gradient in the bedrock (computed on four vertical levels) we compute a heat flux $\phi'_0$ at the ice-bedrock interface. In case of ice dragging over the bedrock, an additional term due to friction, $\phi_f$, is added to $\phi'_0$:

$$\phi_f = |\mathbf{u}_b \, \tau_b| \tag{20}$$

The ice-bedrock interface heat flux is used differently for cold and temperate based points:

- For cold based points, the heat at the ice-bedrock interface is transferred to the ice via a Neumann boundary condition:

$$k_i \frac{\partial T}{\partial z}|_{ice} = -\phi'_0 - \phi_f \tag{21}$$

with the ice thermal conductivity $k_i$ computed as:

$$k_i = 3.1014\ 10^8\ exp(-0.0057\ (T + 273.15)) \tag{22}$$

Geosci. Model Dev. Discuss., https://doi.org/10.5194/gmd-2018-105
Manuscript under review for journal Geosci. Model Dev.
Discussion started: 2 May 2018




– For temperate points, a Dirichlet boundary condition is applied as the temperature is kept at the pressure melting point. The excess heat in this case is used to compute basal melting:

$$b_{melt} = \frac{-\phi_0' - \phi_f - k_i \frac{\partial T}{\partial z}|_{ice}}{L_f \rho_i} \tag{23}$$

with $L_f$ is the latent heat of fusion.

Basal melting for oceanic points is usually imposed. For specific applications we have different values for deep ocean and continental shelves, or a geographical distribution depending on the oceanic basin.

## 2.2 Additional features

### 2.2.1 Basal hydrology

Since the work of Peyaud (2006), GRISLI accounts for a simple diffusive basal hydrology scheme to calculate the water pressure. Using a Darcy law, the water produced by melting at the base of the ice sheet is routed outside glaciated areas following the highest gradient in the total water potential.

Such a gradient can be written as:

$$\nabla\Phi = \nabla p_w + \rho_w g \nabla B + \rho_i g \nabla H \tag{24}$$

where $p_w$ is the water pressure, $B$ is the bedrock height and $H$ the ice thickness.

In GRISLI, water is supposed to flow within a thickness of 20 meters of till with a 50% porosity. Inside the till, assuming a Darcy-type flow law, the water flux $\mathbf{Q}_w$ is proportional to the water potential gradient. For example in the $x$ direction:

$$Q_{wx} = -\frac{K\ D}{\rho_w g}\frac{\partial \Phi}{\partial x} = -\frac{K\ D}{\rho_w g}\frac{\partial}{\partial x}\left(\rho_w g \nabla B + \rho_i g \nabla H\right) - K\ D\frac{\partial h_w}{\partial x} \tag{25}$$

with $h_w$ the hydraulic head and $D$ the water depth in the till. The hydraulic conductivity of the till, $K$, is modulated by the effective pressure to take into account sediment dilatation:

$$K = \begin{cases} K_0 & \text{if } N > N_0 \\ K_0\ N_0/N & \text{if } N \leq N_0 \end{cases} \tag{26}$$

with $K_0$ the reference conductivity, $N$ the effective pressure and $N_0$ a constant ($10^8 Pa$). The conductivity $K_0$ is poorly constrained and strongly depends on the material.

The combination of Eq. 24 and Eq. 25 reduces to a diffusivity equation for the hydraulic head, $h_w$, which ultimately gives the water pressure, $p_w = \rho_w\ g\ h_w$. Similarly to what is done for the mass conservation equation a semi-implicit relaxation method is used to solve the basal hydrology.

### 2.2.2 Isostasy

GRISLI computes the bedrock response to ice load with an elastic lithosphere - relaxed asthenosphere (ELRA) model. This simple model evaluates the bedrock deformation to a local unit mass, scaled to the whole ice sheet. The relaxation time

Geosci. Model Dev. Discuss., https://doi.org/10.5194/gmd-2018-105
Manuscript under review for journal Geosci. Model Dev.
Discussion started: 2 May 2018




of the asthenosphere is usually set to 3000 years and the deflection of the lithosphere is assumed to follow a zero-order Kelvin function. Such a simple model has been shown to perform well compared to more sophisticated glacio-isostatic models (Le Meur and Huybrechts, 1996).

#### 2.2.3 Passive tracer

GRISLI includes a passive tracer model that allows for the computation of vertical ice stratigraphy, i.e. time and location of ice deposition for the vertical model grid points (Lhomme et al., 2005; Quiquet et al., 2013). For this, we use a semi-Lagrangian scheme following Clark and Mix (2002) in order to avoid the numerical instabilities of Eulerian schemes and information dispersion of Lagrangian schemes (Rybak and Huybrechts, 2003). For each timestep, the back trajectories of each grid points are computed and tri-linearly interpolated onto the model grid. This allows for a continuous information within the ice sheet at a low computational cost. Time and location of ice deposition can be convoluted for example with isotopic composition of precipitation (e.g. $\delta^{18}O$) in order to construct synthetic ice cores comparable with actual ice cores (Lhomme et al., 2005).

### 2.3 Numerical features

The model uses finite differences computed on a staggered Arakawa C-grid in the horizontal plane. The model defines $\sigma$-reduced coordinates for 21 evenly spaced vertical layers. The horizontal resolution depends on the application, i.e. the extension of the geographical domain and the duration of the simulated period. For century scale applications, the resolution varies from 5 km for Greenland to 15 km for Antarctica (Peano et al., 2017; Ritz et al., 2015). For multi-millenial applications the resolution increases to 15 km for Greenland and 40 km for the whole Northern Hemisphere and Antarctica. The model uses a main time step ranging from 0.5 to 5 years depending on the horizontal resolution. Based on the maximum magnitude of the simulated velocity over the whole domain, the model computes a shorter time step for the mass conservation equation (Eq. 2) in order to avoid numerical instabilities.

The resolution of the elliptic system (Eq. 12) is the most expensive part of the model. This is further amplified by the fact that, as in Ritz et al. (2001), the ice shelf region is artificially extended towards the edges of the geographical domain in order to get an ice front systematically parallel to either x or y. This artificial extension does not have any consequence on ice shelf velocity since added grid points are prescribed with a negligible ice viscosity ($1500\ Pa\ s$). In order to reduce the size of the linear system solved in Eq. 12, we use a simple reduction method. Eq. 12 can be written as $A\ \mathbf{u} = B$ where $\mathbf{u}$ is a vector alternating $u_x$ and $u_y$ components for all the velocity grid points, $A$ is a band matrix (very sparse) and $B$ is a vector corresponding to the right hand terms in Eq. 12. For a given velocity node (i.e. row $i$ ), if all the terms of column $i$ in matrix A are small except $A_{ii}$, this means that this node is actually not used by any other velocity node. Row $i$ can be therefore removed from the matrix. We use the value of the integrated viscosity of artificial ice shelves ($1500\ Pa\ s$) to define the threshold to neglect nodes. In practice, given its size, the matrix A is not constructed, only the non zero diagonals are.

Geosci. Model Dev. Discuss., https://doi.org/10.5194/gmd-2018-105
Manuscript under review for journal Geosci. Model Dev.
Discussion started: 2 May 2018




The model has been recently partially parallelised with OpenMP, which considerably shortens the length of the simulations (gain of 40% for the Antarctic at 40 km on four threads of an Intel® Xeon® CPU@3.47 GHz ).

## 3 Calibration for the Antartic ice sheet

### 3.1 Methods

Given its degree of complexity, GRISLI is mostly designed for multi-millenial integrations. Due to long-term diffusive response to SMB and temperature changes, an accurate methodology to select unknown parameters of the model would be to run long transient simulations with a climate forcing as close as possible from past climate states, ideally with a synchronous coupling between the ice sheet and the atmosphere. However, climate models generally fail at reproducing the regional climate changes during the last glacial-interglacial cycle as recorded by proxy data (Braconnot et al., 2012). Furthermore, the phase III of the Paleoclimate Modelling Intercomparison Project (PMIP3) has highlighted the large disagreement between participating climate models in simulating the Last Glacial Maxium (LGM) in the vicinity of northern Hemisphere ice sheets (e.g. Harrison et al., 2014). Given these uncertainties amongst climate models and the large sensitivity of the ice sheet model to climate forcing fields (e.g. Charbit et al., 2007; Quiquet et al., 2012; Yan et al., 2013), it is difficult to calibrate the mechanical parameters independently from that of the SMB, in particular for northern Hemisphere ice sheets.

For these reasons, here we suggest a simple calibration methodology for the Antarctic ice sheet in which the model is run for 100 kyrs under a constant climate forcing in order to reach an ice sheet equilibrium. In the following, we use the 27 km-grid atmospheric outputs, namely annual mean temperature and SMB, from the regional climate model RACMO2 2.3 (Noël et al., 2015), averaged over the 1976-2016 time span. The basal melting rates under ice shelves are prescribed for the 18 sectors of the Antarctic ice sheet as defined in ISMIP-Antarctica projet (Fig. 2). Their values are in line with observations-based estimates (Rignot et al., 2013). We do not apply any correction related to geometry changes to the climatic forcings during the calibration.

We choose to restrict this study to a coarse horizontal resolution, namely 40 km, as it allows for large ensembles of multi-millenial simulations. Whilst 6.7 hours on one thread of an Intel® Xeon® CPU@3.47 GHz (4 hours on four threads) are needed to perform 100 000 years of simulation over Antarctica on a 40-km grid (19 881 horizontal grid points), this time goes up significantly on a 16-km grid (145 161 points) for which we need 25 hours to perform 2000 years (17 hours on four threads). In addition, the 40 km resolution corresponds to the one used in the coupled version within the *i*LOVECLIM earth system model of intermediate complexity (Roche et al., 2014). Whilst with such a resolution we do not expect to have an accurate representation of the ice sheet fine scale structures such as ice streams, we expect to reproduce the large scale behaviour of ice flow.

From our experience with GRISLI, we identified four unknown parameters that have a crucial role for ice dynamics and that are independent from each other:

Geosci. Model Dev. Discuss., https://doi.org/10.5194/gmd-2018-105
Manuscript under review for journal Geosci. Model Dev.
Discussion started: 2 May 2018




- The SIA flow enhancement factor $E_{SIA}$ of the Glen flow law (Eq. 9). This coefficient is expected to have a large influence on shear-stress driven velocities.
- The basal drag coefficient $C_f$ in Eq. 14. This coefficient is used to modulate the basal drag coefficient for temperate-based grid points where sliding occurs.
- The till conductivity $K_0$. This parameter changes the efficiency of basal water routing and thus, basal effective pressure. As such, this parameter is also influencing the basal drag coefficient $\beta$ for temperate-based regions.
- An ice shelf basal melting rate coefficient $\phi_{shelf}$. For a specific Antarctic ice shelf sector $i$:

$$BMB^i = \phi_{shelf} BMB_0^i \tag{27}$$

with $BMB_0^i$ the sub-shelf basal melting rate reference values shown in Fig. 2. Whilst the choice of $BMB_0^i$ is based on the sectoral average of sub-shelf melt rates that ensured stable ice shelves in the recent intercomparison exercice InitMIP-Antarctica (Nowicki et al., 2016), with slight modifications due to change in resolution.

The parametric ensemble is designed with a Latin Hypercube Sampling (LHS) methodology. The LHS is used here because it has better space-filling quality than a standard Monte-Carlo sampling which might not explore sufficiently the tails of parameter distributions. This methodology has been used for calibration purposes in the ice sheet modelling community (e.g. Stone et al., 2010; Applegate et al., 2012). The size of the LHS consists in 150 model realisations. We perform two times the entire cube with the flux at the grounding line of Schoof (2007) (hereafter AN40S) and Tsai et al. (2015) (hereafter AN40T) The range of explored parameters are listed in Tab. 2. We assume an uniform statistical distribution within this range.

The initial ice sheet geometry, bedrock and ice thickness, is taken from the Bedmap2 dataset (Fretwell et al., 2013). The geothermal heat flux is from Shapiro and Ritzwoller (2004). Sensitivity to uncertainties in the forcing data are discarded from the ensemble as we aim at quantifying the model sensitivity to parameter choice even though we acknowledge for the fact that these could be the source of important model error (e.g. Stone et al., 2010; Pollard and DeConto, 2012).

### 3.2 Calibration results

Fig. 3 presents the Antarctic ice sheet volumes at the end of the 100 kyr simulations for each ensemble members as a function of parameter values using the flux at the grounding line computed from Schoof (2007) (AN40S). We can see that there is a strong positive (respectively negative) correlation of ice volume with the basal drag coefficient (resp. enhancement factor). There is also a weak negative correlation for the sub-shelf basal melt coefficient. However, there is no correlation with the till conductivity. Since the global volume is an integrated metric that does not account for potential systematic compensation, we computed the root mean square error (RMSE) in ice thickness for each ensemble members with respect to observations (Fretwell et al., 2013). In Fig. 3, the red stars correspond to the ensemble members presenting a RMSE lower than 350 m. 63 model realisations meet this criterion and are widespread across the range of parameter values. The lowest RMSE is 304 m.

Geosci. Model Dev. Discuss., https://doi.org/10.5194/gmd-2018-105
Manuscript under review for journal Geosci. Model Dev.
Discussion started: 2 May 2018




The general model response amongst the ensemble members is not fundamentally different when the flux at the grounding line is computed from Tsai et al. (2015) (Fig. 4). However, the grounding line position is much more unstable with a greater number of members showing lower ice sheet volume. Only 27 model realisations present a RMSE lower than 350 m (lowest RMSE at 298 m), compared to 63 within the AN40S ensemble members. This difference in term of grounding line stability for the two flux formulations has already been highlighted by Pattyn (2017). Since basal drag vanishes at the grounding line in the Tsai et al. (2015) formulation, its coefficient has a smaller impact than in Schoof (2007), amplifying the role of the ice flow enhancement factor. For the AN40T ensemble, this factor requires values between 1.5 and 3 in order to reach a good agreement with observed ice thickness, whilst values within 1.5 to 5 are acceptable for AN40S.

In Fig. 5 (respectively Fig. 6) we show the ice thickness difference from the observations for the 12 ensemble members showing the lowest RMSE within the AN40S (resp. AN40T) model realisations. The differences are generally below 500 m even if persisting model biases are present across the ensemble members and model formulations. On the one hand, ice thickness in large parts of the East Antarctic ice sheet is systematically underestimated. On the other hand, the West Antarctic ice sheet shows more contrasted responses. Whilst for some ensemble members, the Ross embayment upstream region can be well represented (e.g. AN40S004 or AN40T065), the region feeding the Filchner-Ronne ice shelf show a quasi-systematic ice thickness underestimation. These model deficiencies can be attributed to our coarse model resolution, providing a poor representation of the complex bedrock structure in the Filchner-Ronne area. The model differences from the observations are very similar to results from the PISM-PIK model shown in Martin et al. (2011) in term of amplitude but also in term of structure. They are also generally similar to Pollard and DeConto (2009).

Fig. 7 presents the ensemble members in two-dimensional parametric space. The ensemble members depicted in colours are the ones matching the selection criterion within AN40S (red), AN40T (blue) and for both of them (green). In most cases there is no clear relationship. However, there is a relationship emerging with a large basal drag coefficient being compensated by a large enhancement factor when using the Schoof (2007) formulation (red and green stars). When using the Tsai et al. (2015) formulation (blue and green stars), this relationship disappears as the enhancement factor is mostly driving the model response. A few model parameter combinations are able to provide a good representation of the present day Antarctic ice sheet, i.e. low RMSE, independently from the grounding flux computation used.

Although our quality metric is based on the ice sheet thickness we show in Fig 8 and in Fig. 9 the capability of the model to reproduce observed ice sheet velocity (Mouginot et al., 2017) for the best ensemble members with the two formulations of the flux at the grounding line. The model reproduces the general distribution of the velocity although it underestimates ice flow for the very fast grid points (velocity larger than $100\ m\ yr^{-1}$, generally ice shelves). The model has also difficulties to reproduce well-defined ice streams such as the Amery or Filchner ice shelves tributaries. These could be due to the coarse resolution used but also to the simple scheme used to estimate basal drag.

Geosci. Model Dev. Discuss., https://doi.org/10.5194/gmd-2018-105
Manuscript under review for journal Geosci. Model Dev.
Discussion started: 2 May 2018




## 4 Antartic ice sheet changes for the last 400 kyrs

### 4.1 Methods

The main objective of this section is to show the ability of the model to reproduce large ice sheet geometry changes in response to Quaternary climate change. As a consequence of our limited knowledge of past climatic conditions in the Antarctic ice sheet region over glacial-interglacial cycles, we use here an idealised reconstruction of SMB, near surface air temperature and oceanic basal melting rates based on a limited number of proxy records. Our approach is somehow similar to previous works (e.g. Ritz et al., 2001; Huybrechts, 2002; Pollard and DeConto, 2009; Greve et al., 2011; Golledge et al., 2014).

The near-surface air temperature, used in the model as a surface boundary condition for the advection-diffusion temperature equation, is assumed to follow the EPICA-DOMEC deuterium record $\delta D$:

$$T_{palaeo} = T_0 + \left(1/\alpha^i\right) \delta D \tag{28}$$

with $T_0$ the annual mean near-surface air temperature from RACMO2 used for the present-day calibration. The isotopic slope for temperature, $\alpha^i$, is set to $0.18\,‰^{\circ}C^{-1}$ as in (Jouzel et al., 2007).
We also account for the additional temperature perturbation due to topography changes using a fixed and homogeneous lapse rate $\lambda$:

$$T^*_{palaeo} = T_{palaeo} + \lambda\,(S - S_0) \tag{29}$$

with $S - S_0$ the local topography change from Bedmap2. In the following $\lambda$ is set to $-8\,^{\circ}C\;km^{-1}$.

For a given near-surface air temperature change $T^*_{palaeo}$ relative to present-day $T_0$, we modify the present-day SMB field, $SMB_0$:

$$SMB = SMB_0\; exp\left(-\gamma\left(T_0 - T^*_{palaeo}\right)\right) \tag{30}$$

with the precipitation ratio to temperature change $\gamma$ set to $0.07\,^{\circ}C^{-1}$. The use of an exponential form in Eq. 30 is motivated by the Clausius-Clapeyron saturation vapour pressure for an ideal gas. Such a simple expression implies that SMB is driven only by accumulation, an assumption justified by the very little surface ablation experienced by the Antarctic ice sheet under present-day climatic conditions. However, we may underestimate the surface melt for warmer past interglacial periods.

In order to account for changes in basal melting rates below ice shelves, there is the need to define a continuous proxy covering several glacial-interglacial cycles for past sub-surface oceanic conditions around Antarctica. To this end, and due to the lack of such a record in the Southern ocean, we used the temperature derived from a benthic foraminifer $\delta^{18}O$ record from the North Atlantic. This temperature signal is considered to depict the North Atlantic Deep Water (NADW) temperature (Waelbroeck et al., 2002). Here, we assume that changes in NADW temperature drive changes in the temperature of waters upwelled in

Geosci. Model Dev. Discuss., https://doi.org/10.5194/gmd-2018-105
Manuscript under review for journal Geosci. Model Dev.
Discussion started: 2 May 2018




the Southern Ocean. This upward flow separates into surface equatorward and poleward flows, and thus influences surface and sub-surface temperature around coastal Antarctica (e.g. Ferrari et al., 2014). The basal melting rate below a specific ice shelf sector $i$, $BMB^i_{palaeo}$ for past periods is computed from its present-day value, $BMB^i_0$, corrected to account for past oceanic conditions:

$$BMB^i_{palaeo} = max\ \left(BMB^i_0\ (1+\delta^{oc})\ ,\ 0.01\ m\ yr^{-1}\right) \tag{31}$$

using the palaeo-oceanic index $\delta^{oc}$ defined as:

$$\delta^{oc} = \alpha^{oc}\ \Delta T_{NA}/T_{NA0} \tag{32}$$

with $T_{NA0}$ the pre-industrial temperature deduced from North Atlantic benthic foraminifera (Waelbroeck et al., 2002) and $\Delta T_{NA}$ the deviation from this temperature in the past. $\alpha^{oc}$ is a conversion coefficient, set to 1 in the following.
The atmospheric and oceanic indexes, $T_{palaeo} - T_0$ and $\delta^{oc}$, used to drive the model for the last 400 kyr are presented in Fig. 10. In addition to these climatic perturbations we also use the eustatic sea level reconstruction of Waelbroeck et al. (2002) to account for sea level variations over glacial-interglacial cycles.

In the following, we discuss the model behaviour as the result to the 400 kyr forcing. We performed simulations using the 12 parameter combinations from Sec. 3 that yield the lowest RMSE for the two groups AN40S and AN40T, differing by the treatment of the flux at the grounding line. The internal variables at the end of the 100 kyr under present-day constant climate forcing are used as initial conditions for the transient simulations. We artificially expand the simulations for 10 kyr into the future with no climatic perturbation from the reference climate used in Sec. 3 in order to discuss the stability of the simulated present-day ice sheet state.

### 4.2 Transient simulation results

In Fig. 11 the simulated ice sheet volume is shown over the last 400 kyr. Across this time scale, a large glacial-interglacial volume variation is observed, in particular for the last two cycles where it reaches up to about 10 millions of $km^3$. In our simulations, the Antarctic ice sheet volume increase at the last glacial maximum (21 kaBP) relative to pre-industrial corresponds to about -10 to -20 m of global eustatic sea level drop depending on the simulations. These numbers mostly fall in the range of previous ice sheet model reconstructions (e.g. Huybrechts, 2002; Philippon et al., 2006; Pollard and DeConto, 2009), Antarctic contributions inferred as the difference from far-field and Northern Hemisphere near-field estimates (Peltier, 2004) or near-field estimates (Ivins and James, 2005; Argus et al., 2014; Whitehouse et al., 2012; Briggs et al., 2014). In our simulations, the last interglacial (120 kaBP) ice volume does not present substantial changes relative to the present-day ice volume, as the Antarctic ice sheet is contributing to less than 6 centimetres to the global eustatic sea level rise in the simulations with the lowest RMSE at 0k. This is well below recent estimates, ranging from 3 to 7 m, inferred from the limited contribution of Greenland to the last interglacial highstand (Dutton et al., 2015). Our crude representation of the last interglacial climate in which no surface melt is possible may be the cause for such a discrepancy. In addition, our proxy-based basal melting rate does not allow for above

Geosci. Model Dev. Discuss., https://doi.org/10.5194/gmd-2018-105
Manuscript under review for journal Geosci. Model Dev.
Discussion started: 2 May 2018




than present basal melting rates during the last interglacial.

The uncertainty related to the choice of the internal parameters leads generally to up to 3 $10^6$ $km^3$ differences in our framework but do not change the model response to the forcings. In turns, the choice of either Schoof (2007) (AN40S) or Tsai et al. (2015) (AN40T) to compute the flux at the grounding line leads to important differences amongst temporal model responses. AN40T systematically start to retreat before AN40S. It also produces a larger glacial to interglacial volume changes. This confirms the fact that the Tsai et al. (2015) formulation leads to more sensitive grounding line already highlighted in Sec. 3 and by other authors (Pattyn, 2017). The additional 10 kyr into the future with no climatic perturbation shows that the AN40S ensemble members do not produce an ice sheet at equilibrium at 0 ka BP. This means that, in our model, the Schoof (2007) formulation produces unrealistically too slow retreat which induces a model drift persisting till 10 kyr in the future. Conversely, the Tsai et al. (2015) formulation leads to more rapid retreat rates which provides a stabilisation of the ice sheet during the Holocene.

Simulated ice sheet surface elevations at selected snapshots for the two ensemble members with the lowest RMSE at 0 ka BP after the transient simulations are presented in Fig. 12. Ice sheet geometry during the last interglacial resembles the present-day one. This is particularly true for the eastern part whilst the West Antarctic ice sheet is only slightly thinner. At the last glacial maximum, the grounding line advances towards the edge of the continental shelf, in agreement with geological reconstructions (Bentley et al., 2014). The choice of the flux at the grounding line formulation has an impact on the maximum ice sheet extent, with a less extended ice sheet using the Schoof (2007) formulation. As for the last interglacial, the eastern part of the ice sheet presents only small variations in surface elevation compared to the present-day geometry. There is no decrease in surface elevation at the last glacial maximum due to reduction in precipitation at this time since the larger extent and the colder climate tend to reduce the ice flow. The largest topography changes are occurring in the Weddel and Ross sea. The West Antarctic ice sheet is thus particularly dynamic during glacial-interglacial cycles.

The RMSE computed at 0 ka BP for the 24 members used for the transient simulations ranges from 372 to 467 m within AN40S and 326 to 376 m within AN40T. These numbers are only slightly greater than the ones obtained using a constant forcing (Sec. 3). The differences in ice sheet thickness between the transient simulations at 0 ka BP and the observations for the two ensemble members with the lowest RMSE (AN40S097 and AN40T059) are shown in Fig. 13. The pattern is similar to the one obtained during the calibration step (Sec. 3) with some notable differences. On the one hand, the East Antarctic ice sheet thickness underestimation is partly corrected when performing a transient simulation. This could be the result of a better representation of the temperature vertical profile in this case. On the other hand, whilst in other regions the model biases remain generally the same between an equilibrium and a transient simulation, important model biases appear at the margins of the ice sheet when using the transient simulations. This is particularly visible when using Schoof (2007) for which the retreat rate during the deglaciation is underestimated. Part of the misrepresentation of present-day margins could also be due to the over-simplified climatic perturbation used for the transient simulations.

Geosci. Model Dev. Discuss., https://doi.org/10.5194/gmd-2018-105
Manuscript under review for journal Geosci. Model Dev.
Discussion started: 2 May 2018




## 5 Discussion and outlook

We have presented results from the updated version of the GRISLI model. Whilst the model is able to reproduce present-day Greenland (Le clec'h et al., 2017) and Antarctic (Ritz et al., 2015) ice sheets when using an inverse method to estimate the basal drag, our simulations show some important disagreements relative to observations. In particular there are some persisting model biases in ice thickness: underestimation (resp. overestimation) of southern (resp. northern) part of East Antarctic and underestimation (resp. overestimation) of Ronnie-Filchner (resp. Ross) basins. These model biases are also present in models of similar complexity when using an interactive basal drag computation (Pollard and DeConto, 2009; Martin et al., 2011). This data-model mismatch is mostly due to a poor representation of the bedrock-ice interface. In particular, the coarse resolution does not allow for the consideration of fine scale troughs and pinning points. The persisting model biases can be also the consequence of our simplified basal drag computation that does not take into account bedrock physical properties (e.g. sediments).

We used a basal drag computed from an internal model parameter, namely the basal effective pressure. For long-term multi-millenial integrations, this is preferred to basal drag deduced from inversion using present-day geometry since it is fully consistent with the model physics and, in principle, remains valid for large ice sheet geometry change. However, by design, the fit with observations is systematically poorer compared to results from inversion. A step forward would be to use the basal drag computed from inversion in order to infer a formulation based solely on internal parameters. Amongst these parameters, the large scale bedrock curvature and/or sub-grid roughness could be used, similarly to Briggs et al. (2013). To progress further on this topic, the implementation of a new basal hydrology model relying on explicit routing scheme (e.g. Kavanagh and Tarasov, 2017) would allow to avoid relaxed numerical solutions based on effective pressure. This could introduce fast basal water changes that are currently ignored and, ultimately, could yield ice streams abrupt speed-up or slow-down.

Although widely used for ice sheet model spin-up or calibration, long-term integrations under present-day forcing induce misrepresentation of the vertical temperature profile. Calibrated parameters obtained with such a methodology tend to compensate for the under-estimated viscosity and are in theory not suitable for palaeo-reconstructions. Whilst a parameter calibration based on glacial-interglacial simulations is ideally preferred, the determination of a realistic climate forcing is a considerable challenge given the many degrees of freedom. Here, we presented a very simplified climate reconstructions for the last 400 kyr based on a minimal parameter set (proxy for atmospheric temperatures and oceanic conditions) in order to illustrate the model possible behaviour for long-term integrations. Further work will consist in the determination of more realistic climate reconstruction using general circulation model snapshots. We also aim at expanding the work of Roche et al. (2014) and couple the Antarctic geometry of GRISLI version 2.0 with the *i*LOVECLIM model.

The implementation of an explicit flux computation at the grounding line following Schoof (2007) and Tsai et al. (2015) lead to a more unstable position of the grounding line compared to previous version of the model. As such, GRISLI version 2.0 is now more sensitive to change in sea level. However, the current version of the model only considers an eustatic sea level



perturbation with a regional bedrock adjustment. The explicit computation of local relative sea level could potentially have an important impact on grounding line migration for glacial-interglacial cycles (e.g. Gomez et al., 2013).

Calving processes are suspected to be a major driver for ice sheet evolution due to the importance of buttressing on inland ice dynamics (e.g. Pollard et al., 2015). GRISLI v2 includes a very simplified calving representation that might prevent to assess the role of this process for multi-millenial ice dynamics. The inclusion of a physically based calving scheme (e.g. Christmann et al., 2016) would be a significant model improvement for future model revisions.

## 6 Conclusions

We have presented the GRISLI (version 2.0) model along with the significant improvements from the previous version of Ritz et al. (2001). Such improvements include an explicit flux computation at the grounding line, an interactive basal hydrology module and a semi-lagrangian tracking particle scheme. Thanks to its low computational cost, the model is suitable for long-term multi-millenial integrations. We performed a large ensemble of simulations of the Antarctic ice sheet forced by present-day climate conditions to calibrate the crucial unknown parameters. We have shown that the model is able to reproduce reasonably well the present-day geometry although the grounding line position in the model is much more unstable when we use Tsai et al. (2015) formulation of the flux at the grounding line instead of Schoof (2007). The model mismatch with respect to observed ice thickness shows some systematic biases (e.g. the East Antarctic ice sheet is too thick in the vicinity of the Transantarctic mountains and too thin elsewhere), that are similar to models of comparable complexity. We used the best ensemble members to simulate the Antarctic evolution throughout the last 400 kyr using an idealised climatic perturbation of present-day conditions. With this simple framework we reproduced the expected ice sheet geometry changes over glacial-interglacial cycles. A significant volume increase is simulated during glacial periods with a grounding line advance towards the edge of the continental shelf. The retreat during terminations is gradual when using our forcing scenario and is able to produce a final present-day ice volume and extent similar to observations. The Tsai et al. (2015) formulation produces a faster ice sheet retreat and yields an ice sheet near equilibrium during the Holocene contrary to Schoof (2007) for which the model is still drifting at +10 kyr into the future. This suggests that, in our model, the Tsai et al. (2015) formulation produces a more realistic grounding line retreat rate. The validation of the model for the Antarctic ice sheet changes through glacial-interglacial cycles give confidence in ice dynamics in the model and its applicability to northern Hemisphere ice sheets.

## 7 Code availability

The developments on the GRISLI source code are hosted at https://forge.ipsl.jussieu.fr/grisli, but are not publicly available due to copyright restrictions. Access can be granted on demand by request to Catherine Ritz (catherine.ritz@univ-grenoble-alpes.fr), Christophe Dumas (christophe.dumas@lsce.ipsl.fr) and Aurélien Quiquet (aurelien.quiquet@lsce.ipsl.fr) to those who conduct research in collaboration with the GRISLI users group. For this work we used the model at revision 188.

Geosci. Model Dev. Discuss., https://doi.org/10.5194/gmd-2018-105
Manuscript under review for journal Geosci. Model Dev.
Discussion started: 2 May 2018


*Acknowledgements.* We thank Michiel van den Broeke (IMAU, Utrecht University) for providing the RACMO2 2.3 model outputs. We also warmly thank Claire Waelbroeck for fruitful discussions on the construction of the index for sub-shelf melting rates. This is a contribution to ERC project ACCLIMATE; the research leading to these results has received funding from the European Research Council under the European Union's Seventh Framework Programme (FP7/2007-2013)/ERC grant agreement 339108.



## References

Abe-Ouchi, A., Saito, F., Kawamura, K., Raymo, M. E., Okuno, J., Takahashi, K., and Blatter, H.: Insolation-driven 100,000-year glacial cycles and hysteresis of ice-sheet volume, Nature, 500, 190–193, doi:10.1038/nature12374, 2013.

Alvarez-Solas, J., Charbit, S., Ritz, C., Paillard, D., Ramstein, G., and Dumas, C.: Links between ocean temperature and iceberg discharge during Heinrich events, Nature Geosci, 3, 122–126, doi:10.1038/ngeo752, 2010.

Alvarez-Solas, J., Robinson, A., Montoya, M., and Ritz, C.: Iceberg discharges of the last glacial period driven by oceanic circulation changes, Proceedings of the National Academy of Sciences, 110, 16 350–16 354, doi:10.1073/pnas.1306622110, 2013.

Applegate, P. J., Kirchner, N., Stone, E. J., Keller, K., and Greve, R.: An assessment of key model parametric uncertainties in projections of Greenland Ice Sheet behavior, The Cryosphere, 6, 589–606, doi:10.5194/tc-6-589-2012, 2012.

Argus, D. F., Peltier, W. R., Drummond, R., and Moore, A. W.: The Antarctica component of postglacial rebound model ICE-6G_C (VM5a) based on GPS positioning, exposure age dating of ice thicknesses, and relative sea level histories, Geophysical Journal International, 198, 537–563, doi:10.1093/gji/ggu140, 2014.

Benn, D. I., Le Hir, G., Bao, H., Donnadieu, Y., Dumas, C., Fleming, E. J., Hambrey, M. J., McMillan, E. A., Petronis, M. S., Ramstein, G., Stevenson, C. T. E., Wynn, P. M., and Fairchild, I. J.: Orbitally forced ice sheet fluctuations during the Marinoan Snowball Earth glaciation, Nature Geoscience, 8, 704–707, doi:10.1038/ngeo2502, 2015.

Bentley, M. J., Ó Cofaigh, C., Anderson, J. B., Conway, H., Davies, B., Graham, A. G. C., Hillenbrand, C.-D., Hodgson, D. A., Jamieson, S. S. R., Larter, R. D., Mackintosh, A., Smith, J. A., Verleyen, E., Ackert, R. P., Bart, P. J., Berg, S., Brunstein, D., Canals, M., Colhoun, E. A., Crosta, X., Dickens, W. A., Domack, E., Dowdeswell, J. A., Dunbar, R., Ehrmann, W., Evans, J., Favier, V., Fink, D., Fogwill, C. J., Glasser, N. F., Gohl, K., Golledge, N. R., Goodwin, I., Gore, D. B., Greenwood, S. L., Hall, B. L., Hall, K., Hedding, D. W., Hein, A. S., Hocking, E. P., Jakobsson, M., Johnson, J. S., Jomelli, V., Jones, R. S., Klages, J. P., Kristoffersen, Y., Kuhn, G., Leventer, A., Licht, K., Lilly, K., Lindow, J., Livingstone, S. J., Massé, G., McGlone, M. S., McKay, R. M., Melles, M., Miura, H., Mulvaney, R., Nel, W., Nitsche, F. O., O'Brien, P. E., Post, A. L., Roberts, S. J., Saunders, K. M., Selkirk, P. M., Simms, A. R., Spiegel, C., Stolldorf, T. D., Sugden, D. E., van der Putten, N., van Ommen, T., Verfaillie, D., Vyverman, W., Wagner, B., White, D. A., Witus, A. E., and Zwartz, D.: A community-based geological reconstruction of Antarctic Ice Sheet deglaciation since the Last Glacial Maximum, Quaternary Science Reviews, 100, 1–9, doi:10.1016/j.quascirev.2014.06.025, 2014.

Bindschadler, R.: The Importance of Pressurized Subglacial Water in Separation and Sliding at the Glacier Bed, Journal of Glaciology, 29, 3–19, doi:10.3189/S0022143000005104, 1983.

Braconnot, P., Harrison, S. P., Kageyama, M., Bartlein, P. J., Masson-Delmotte, V., Abe-Ouchi, A., Otto-Bliesner, B., and Zhao, Y.: Evaluation of climate models using palaeoclimatic data, Nature Climate Change, 2, 417–424, doi:10.1038/nclimate1456, 2012.

Briggs, R., Pollard, D., and Tarasov, L.: A glacial systems model configured for large ensemble analysis of Antarctic deglaciation, The Cryosphere, 7, 1949–1970, doi:10.5194/tc-7-1949-2013, 2013.

Briggs, R. D., Pollard, D., and Tarasov, L.: A data-constrained large ensemble analysis of Antarctic evolution since the Eemian, Quaternary Science Reviews, 103, 91–115, doi:10.1016/j.quascirev.2014.09.003, 2014.

Bueler, E. and Brown, J.: Shallow shelf approximation as a "sliding law" in a thermomechanically coupled ice sheet model, Journal of Geophysical Research: Earth Surface, 114, F03 008, doi:10.1029/2008JF001179, 2009.

Calov, R., Greve, R., Abe-Ouchi, A., Bueler, E., Huybrechts, P., Johnson, J. V., Pattyn, F., Pollard, D., Ritz, C., Saito, F., and Tarasov, L.: Results from the Ice-Sheet Model Intercomparison Project–Heinrich Event Intercomparison (ISMIP HEINO), Journal of Glaciology, 56, 371–383, doi:10.3189/002214310792447789, 2010.

Charbit, S., Ritz, C., Philippon, G., Peyaud, V., and Kageyama, M.: Numerical reconstructions of the Northern Hemisphere ice sheets through the last glacial-interglacial cycle, Climate of the Past, 3, 15–37, doi:10.5194/cp-3-15-2007, 2007.

Christmann, J., Plate, C., Müller, R., and Humbert, A.: Viscous and viscoelastic stress states at the calving front of Antarctic ice shelves, Annals of Glaciology, 57, 10–18, doi:10.1017/aog.2016.18, 2016.

Clark, P. U. and Mix, A. C.: Ice sheets and sea level of the Last Glacial Maximum, Quaternary Science Reviews, 21, 1–7, doi:10.1016/S0277-3791(01)00118-4, 2002.

Colleoni, F., Kirchner, N., Niessen, F., Quiquet, A., and Liakka, J.: An East Siberian ice shelf during the Late Pleistocene glaciations: Numerical reconstructions, Quaternary Science Reviews, 147, 148–163, doi:10.1016/j.quascirev.2015.12.023, 2016.

Deschamps, P., Durand, N., Bard, E., Hamelin, B., Camoin, G., Thomas, A. L., Henderson, G. M., Okuno, J., and Yokoyama, Y.: Ice-sheet collapse and sea-level rise at the Bølling warming 14,600 years ago, Nature, 483, 559, doi:10.1038/nature10902, 2012.

Donnadieu, Y., Dromart, G., Goddéris, Y., Pucéat, E., Brigaud, B., Dera, G., Dumas, C., and Olivier, N.: A mechanism for brief glacial episodes in the Mesozoic greenhouse, Paleoceanography, 26, PA3212, doi:10.1029/2010PA002100, 2011.

Dumas, C.: Modélisation de l'évolution de l'Antarctique depuis le dernier cycle glaciaire-interglaciaire jusqu'au futur : importance relative des différents processus physiques et rôle des données d'entrée, Ph.D. thesis, Université Joseph-Fourier - Grenoble I, 2002.

Durand, G., Gagliardini, O., de Fleurian, B., Zwinger, T., and Le Meur, E.: Marine ice sheet dynamics: Hysteresis and neutral equilibrium, Journal of Geophysical Research: Earth Surface, 114, F03 009, doi:10.1029/2008JF001170, 2009.

Dutton, A., Carlson, A. E., Long, A. J., Milne, G. A., Clark, P. U., DeConto, R., Horton, B. P., Rahmstorf, S., and Raymo, M. E.: Sea-level rise due to polar ice-sheet mass loss during past warm periods, Science, 349, aaa4019, doi:10.1126/science.aaa4019, 2015.

Duval, P. and Lliboutry, L.: Superplasticity owing to grain growth in polar ices, Journal of Glaciology, 31, 60–62, 1985.

Edwards, T. L., Fettweis, X., Gagliardini, O., Gillet-Chaulet, F., Goelzer, H., Gregory, J. M., Hoffman, M., Huybrechts, P., Payne, A. J., Perego, M., Price, S., Quiquet, A., and Ritz, C.: Effect of uncertainty in surface mass balance–elevation feedback on projections of the future sea level contribution of the Greenland ice sheet, The Cryosphere, 8, 195–208, doi:10.5194/tc-8-195-2014, 2014.

Fairbanks, R. G.: A 17,000-year glacio-eustatic sea level record: influence of glacial melting rates on the Younger Dryas event and deep-ocean circulation, Nature, 342, 637, doi:10.1038/342637a0, 1989.

Favier, L., Durand, G., Cornford, S. L., Gudmundsson, G. H., Gagliardini, O., Gillet-Chaulet, F., Zwinger, T., Payne, A. J., and Brocq, A. M. L.: Retreat of Pine Island Glacier controlled by marine ice-sheet instability, Nature Climate Change, 4, 117, doi:10.1038/nclimate2094, 2014.

Ferrari, R., Jansen, M. F., Adkins, J. F., Burke, A., Stewart, A. L., and Thompson, A. F.: Antarctic sea ice control on ocean circulation in present and glacial climates, Proceedings of the National Academy of Sciences, 111, 8753–8758, doi:10.1073/pnas.1323922111, 2014.

Fretwell, P., Pritchard, H. D., Vaughan, D. G., Bamber, J. L., Barrand, N. E., Bell, R., Bianchi, C., Bingham, R. G., Blankenship, D. D., Casassa, G., Catania, G., Callens, D., Conway, H., Cook, A. J., Corr, H. F. J., Damaske, D., Damm, V., Ferraccioli, F., Forsberg, R., Fujita, S., Gim, Y., Gogineni, P., Griggs, J. A., Hindmarsh, R. C. A., Holmlund, P., Holt, J. W., Jacobel, R. W., Jenkins, A., Jokat, W., Jordan, T., King, E. C., Kohler, J., Krabill, W., Riger-Kusk, M., Langley, K. A., Leitchenkov, G., Leuschen, C., Luyendyk, B. P., Matsuoka, K., Mouginot, J., Nitsche, F. O., Nogi, Y., Nost, O. A., Popov, S. V., Rignot, E., Rippin, D. M., Rivera, A., Roberts, J., Ross, N., Siegert, M. J., Smith, A. M., Steinhage, D., Studinger, M., Sun, B., Tinto, B. K., Welch, B. C., Wilson, D., Young, D. A., Xiangbin, C., and Zirizzotti,

A.: Bedmap2: improved ice bed, surface and thickness datasets for Antarctica, The Cryosphere, 7, 375–393, doi:10.5194/tc-7-375-2013, 2013.

Fürst, J.: Dynamic response of the Greenland ice sheet to future climatic warming, Ph.D. thesis, Vrije Universiteit Brussel, Brussel, 2013.

Gillet-Chaulet, F., Gagliardini, O., Seddik, H., Nodet, M., Durand, G., Ritz, C., Zwinger, T., Greve, R., and Vaughan, D. G.: Greenland ice sheet contribution to sea-level rise from a new-generation ice-sheet model, The Cryosphere, 6, 1561–1576, doi:10.5194/tc-6-1561-2012, 2012.

Goelzer, H., Nowicki, S., Edwards, T., Beckley, M., Abe-Ouchi, A., Aschwanden, A., Calov, R., Gagliardini, O., Gillet-Chaulet, F., Golledge, N. R., Gregory, J., Greve, R., Humbert, A., Huybrechts, P., Kennedy, J. H., Larour, E., Lipscomb, W. H., Le clec´h, S., Lee, V., Morlighem, M., Pattyn, F., Payne, A. J., Rodehacke, C., Rückamp, M., Saito, F., Schlegel, N., Seroussi, H., Shepherd, A., Sun, S., van de Wal, R., and Ziemen, F. A.: Design and results of the ice sheet model initialisation experiments initMIP-Greenland: an ISMIP6 intercomparison, The Cryosphere Discuss., 2017, 1–42, doi:10.5194/tc-2017-129, 2017.

Golledge, N. R., Menviel, L., Carter, L., Fogwill, C. J., England, M. H., Cortese, G., and Levy, R. H.: Antarctic contribution to meltwater pulse 1A from reduced Southern Ocean overturning, Nature Communications, 5, 5107, doi:10.1038/ncomms6107, 2014.

Gomez, N., Pollard, D., and Mitrovica, J. X.: A 3-D coupled ice sheet – sea level model applied to Antarctica through the last 40 ky, Earth and Planetary Science Letters, 384, 88–99, doi:10.1016/j.epsl.2013.09.042, 2013.

Gregoire, L. J., Payne, A. J., and Valdes, P. J.: Deglacial rapid sea level rises caused by ice-sheet saddle collapses, Nature, 487, 219, doi:10.1038/nature11257, 2012.

Greve, R., Saito, F., and Abe-Ouchi, A.: Initial results of the SeaRISE numerical experiments with the models SICOPOLIS and IcIES for the Greenland ice sheet, Annals of Glaciology, 52, 23–30, doi:10.3189/172756411797252068, 2011.

Hall, D. K., Comiso, J. C., DiGirolamo, N. E., Shuman, C. A., Box, J. E., and Koenig, L. S.: Variability in the surface temperature and melt extent of the Greenland ice sheet from MODIS, Geophysical Research Letters, 40, 2114–2120, doi:10.1002/grl.50240, 2013.

Hanebuth, T., Stattegger, K., and Grootes, P. M.: Rapid Flooding of the Sunda Shelf: A Late-Glacial Sea-Level Record, Science, 288, 1033–1035, doi:10.1126/science.288.5468.1033, 2000.

Harrison, S. P., Bartlein, P. J., Brewer, S., Prentice, I. C., Boyd, M., Hessler, I., Holmgren, K., Izumi, K., and Willis, K.: Climate model benchmarking with glacial and mid-Holocene climates, Climate Dynamics, 43, 671–688, doi:10.1007/s00382-013-1922-6, 2014.

Hindmarsh, R. C. A.: A numerical comparison of approximations to the Stokes equations used in ice sheet and glacier modeling, Journal of Geophysical Research: Earth Surface, 109, F01 012, doi:10.1029/2003JF000065, 2004.

Hutter, K.: A mathematical model of polythermal glaciers and ice sheets, Geophysical & Astrophysical Fluid Dynamics, 21, 201–224, doi:10.1080/03091928208209013, 1982.

Hutter, K.: Theoretical glaciology: material science of ice and the mechanics of glaciers and ice sheets, Springer, 1983.

Huybrechts, P.: Sea-level changes at the LGM from ice-dynamic reconstructions of the Greenland and Antarctic ice sheets during the glacial cycles, Quaternary Science Reviews, 21, 203–231, doi:10.1016/S0277-3791(01)00082-8, 2002.

Ivins, E. R. and James, T. S.: Antarctic glacial isostatic adjustment: a new assessment, Antarctic Science, 17, 541–553, doi:10.1017/S0954102005002968, 2005.

Jouzel, J., Masson-Delmotte, V., Cattani, O., Dreyfus, G., Falourd, S., Hoffmann, G., Minster, B., Nouet, J., Barnola, J. M., Chappellaz, J., Fischer, H., Gallet, J. C., Johnsen, S., Leuenberger, M., Loulergue, L., Luethi, D., Oerter, H., Parrenin, F., Raisbeck, G., Raynaud, D., Schilt, A., Schwander, J., Selmo, E., Souchez, R., Spahni, R., Stauffer, B., Steffensen, J. P., Stenni, B., Stocker, T. F., Tison, J. L.,

Werner, M., and Wolff, E. W.: Orbital and Millennial Antarctic Climate Variability over the Past 800,000 Years, Science, 317, 793–796, doi:10.1126/science.1141038, 2007.

Kavanagh, M. and Tarasov, L.: BrAHMs V1.0: A fast, physically-based subglacial hydrology model for continental-scale application, Geosci. Model Dev. Discuss., 2017, 1–20, doi:10.5194/gmd-2017-275, 2017.

Koenig, S. J., Dolan, A. M., de Boer, B., Stone, E. J., Hill, D. J., DeConto, R. M., Abe-Ouchi, A., Lunt, D. J., Pollard, D., Quiquet, A., Saito, F., Savage, J., and van de Wal, R.: Ice sheet model dependency of the simulated Greenland Ice Sheet in the mid-Pliocene, Climate of the Past, 11, 369–381, doi:10.5194/cp-11-369-2015, 2015.

Ladant, J.-B., Donnadieu, Y., Lefebvre, V., and Dumas, C.: The respective role of atmospheric carbon dioxide and orbital parameters on ice sheet evolution at the Eocene-Oligocene transition, Paleoceanography, 29, 2013PA002 593, doi:10.1002/2013PA002593, 2014.

Larour, E., Seroussi, H., Morlighem, M., and Rignot, E.: Continental scale, high order, high spatial resolution, ice sheet modeling using the Ice Sheet System Model (ISSM), Journal of Geophysical Research: Earth Surface, 117, F01 022, doi:10.1029/2011JF002140, 2012.

Le clec'h, S., Fettweis, X., Quiquet, A., Dumas, C., Kageyama, M., Charbit, S., Wyard, C., and Ritz, C.: Assessment of the Greenland ice sheet – atmosphere feedbacks for the next century with a regional atmospheric model fully coupled to an ice sheet model, The Cryosphere Discuss., 2017, 1–31, doi:10.5194/tc-2017-230, 2017.

Le clec'h, S., Quiquet, A., Charbit, S., Dumas, C., Kageyama, M., and Ritz, C.: A rapidly converging spin-up method for the present-day Greenland ice sheet using the GRISLI ice-sheet model, Geosci. Model Dev. Discuss., 2018, 1–21, doi:10.5194/gmd-2017-322, 2018.

Le Meur, E. and Huybrechts, P.: A comparison of different ways of dealing with isostasy: examples from modeling the Antarctic ice sheet during the last glacial cycle, Annals of Glaciology, 23, 309–317, 1996.

Lhomme, N., Clarke, G. K., and Marshall, S. J.: Tracer transport in the Greenland Ice Sheet: constraints on ice cores and glacial history, Quaternary Science Reviews, 24, 173–194, doi:10.1016/j.quascirev.2004.08.020, 2005.

Ma, Y., Gagliardini, O., Ritz, C., Gillet-Chaulet, F., Durand, G., and Montagnat, M.: Enhancement factors for grounded ice and ice shelves inferred from an anisotropic ice-flow model, Journal of Glaciology, 56, 805–812, doi:10.3189/002214310794457209, 2010.

MacAyeal, D. R.: Large-Scale Ice Flow Over a Viscous Basal Sediment: Theory and Application to Ice Stream B, Antarctica, Journal of Geophysical Research, 94, pp. 4071–4087, doi:198910.1029/JB094iB04p04071, 1989.

Martin, M. A., Winkelmann, R., Haseloff, M., Albrecht, T., Bueler, E., Khroulev, C., and Levermann, A.: The Potsdam Parallel Ice Sheet Model (PISM-PIK) – Part 2: Dynamic equilibrium simulation of the Antarctic ice sheet, The Cryosphere, 5, 727–740, doi:10.5194/tc-5-727-2011, 2011.

Mouginot, J., Rignot, E., Scheuchl, B., Fenty, I., Khazendar, A., Morlighem, M., Buzzi, A., and Paden, J.: Fast retreat of Zachariæ Isstrøm, northeast Greenland, Science, 350, 1357–1361, doi:10.1126/science.aac7111, 2015.

Mouginot, J., Rignot, E., Scheuchl, B., and Millan, R.: Comprehensive Annual Ice Sheet Velocity Mapping Using Landsat-8, Sentinel-1, and RADARSAT-2 Data, Remote Sensing, 9, 364, doi:10.3390/rs9040364, 2017.

Nowicki, S. M. J., Payne, A., Larour, E., Seroussi, H., Goelzer, H., Lipscomb, W., Gregory, J., Abe-Ouchi, A., and Shepherd, A.: Ice Sheet Model Intercomparison Project (ISMIP6) contribution to CMIP6, Geosci. Model Dev., 9, 4521–4545, doi:10.5194/gmd-9-4521-2016, 2016.

Noël, B., van de Berg, W. J., van Meijgaard, E., Kuipers Munneke, P., van de Wal, R. S. W., and van den Broeke, M. R.: Evaluation of the updated regional climate model RACMO2.3: summer snowfall impact on the Greenland Ice Sheet, The Cryosphere, 9, 1831–1844, doi:10.5194/tc-9-1831-2015, 2015.

Paolo, F. S., Fricker, H. A., and Padman, L.: Volume loss from Antarctic ice shelves is accelerating, Science, 348, 327–331, doi:10.1126/science.aaa0940, 2015.

Pattyn, F.: Sea-level response to melting of Antarctic ice shelves on multi-centennial timescales with the fast Elementary Thermomechanical Ice Sheet model (f.ETISh v1.0), The Cryosphere, 11, 1851–1878, doi:10.5194/tc-11-1851-2017, 2017.

Peano, D., Colleoni, F., Quiquet, A., and Masina, S.: Ice flux evolution in fast flowing areas of the Greenland ice sheet over the 20th and 21st centuries, Journal of Glaciology, 63, 499–513, doi:10.1017/jog.2017.12, 2017.

Peltier, W. R.: GLOBAL GLACIAL ISOSTASY AND THE SURFACE OF THE ICE-AGE EARTH: The ICE-5G (VM2) Model and GRACE, Annual Review of Earth and Planetary Sciences, 32, 111–149, doi:10.1146/annurev.earth.32.082503.144359, 2004.

Pettit, E. C. and Waddington, E. D.: Ice flow at low deviatoric stress, Journal of Glaciology, 49, 359–369, doi:10.3189/172756503781830584, 2003.

Peyaud, V.: Rôle de la dynamique des calottes glaciaires dans les grands changements climatiques des périodes glaciaires-interglaciaires., Ph.D. thesis, Université Joseph-Fourier - Grenoble I, 2006.

Peyaud, V., Ritz, C., and Krinner, G.: Modelling the Early Weichselian Eurasian Ice Sheets: role of ice shelves and influence of ice-dammed lakes, Climate of the Past, 3, 375–386, doi:10.5194/cp-3-375-2007, 2007.

Philippon, G., Ramstein, G., Charbit, S., Kageyama, M., Ritz, C., and Dumas, C.: Evolution of the Antarctic ice sheet throughout the last deglaciation: A study with a new coupled climate–north and south hemisphere ice sheet model, Earth and Planetary Science Letters, 248, 750–758, doi:10.1016/j.epsl.2006.06.017, 2006.

Pimienta, P.: Etude du comportement mécanique des glaces polychristallines aux faibles contraintes ; applications aux glaces des calottes polaires, thèse, Université Joseph-Fourier - Grenoble I, 1987.

Pollard, D. and DeConto, R. M.: Modelling West Antarctic ice sheet growth and collapse through the past five million years, Nature, 458, 329–332, doi:10.1038/nature07809, 2009.

Pollard, D. and DeConto, R. M.: Description of a hybrid ice sheet-shelf model, and application to Antarctica, Geosci. Model Dev., 5, 1273–1295, doi:10.5194/gmd-5-1273-2012, 2012.

Pollard, D., DeConto, R. M., and Alley, R. B.: Potential Antarctic Ice Sheet retreat driven by hydrofracturing and ice cliff failure, Earth and Planetary Science Letters, 412, 112–121, doi:10.1016/j.epsl.2014.12.035, 2015.

Pritchard, H. D., Arthern, R. J., Vaughan, D. G., and Edwards, L. A.: Extensive dynamic thinning on the margins of the Greenland and Antarctic ice sheets, Nature, 461, 971–975, 2009.

Quiquet, A., Punge, H. J., Ritz, C., Fettweis, X., Gallée, H., Kageyama, M., Krinner, G., Salas y Mélia, D., and Sjolte, J.: Sensitivity of a Greenland ice sheet model to atmospheric forcing fields, The Cryosphere, 6, 999–1018, doi:10.5194/tc-6-999-2012, 2012.

Quiquet, A., Ritz, C., Punge, H. J., and Salas y Mélia, D.: Greenland ice sheet contribution to sea level rise during the last interglacial period: a modelling study driven and constrained by ice core data, Clim. Past, 9, 353–366, doi:10.5194/cp-9-353-2013, 2013.

Rignot, E., Jacobs, S., Mouginot, J., and Scheuchl, B.: Ice-Shelf Melting Around Antarctica, Science, 341, 266–270, doi:10.1126/science.1235798, 2013.

Ritz, C.: Un modèle thermo-mécanique d'èvolution pour le bassin glaciaire antarctique Vostok-Glacier Byrd: Sensibilité aux valeurs des paramètres mal connus, thèse, Université Joseph-Fourier - Grenoble I, 1992.

Ritz, C., Fabre, A., and Letréguilly, A.: Sensitivity of a Greenland ice sheet model to ice flow and ablation parameters: consequences for the evolution through the last climatic cycle, Climate Dynamics, 13, 11–23, doi:10.1007/s003820050149, 1997.

Ritz, C., Rommelaere, V., and Dumas, C.: Modeling the evolution of Antarctic ice sheet over the last 420,000 years: Implications for altitude changes in the Vostok region, Journal of Geophysical Research, 106, 31 943–31 964, doi:10.1029/2001JD900232, 2001.

Ritz, C., Edwards, T. L., Durand, G., Payne, A. J., Peyaud, V., and Hindmarsh, R. C. A.: Potential sea-level rise from Antarctic ice-sheet instability constrained by observations, Nature, 528, 115–118, doi:10.1038/nature16147, 2015.

Roche, D. M., Dumas, C., Bügelmayer, M., Charbit, S., and Ritz, C.: Adding a dynamical cryosphere to iLOVECLIM (version 1.0): coupling with the GRISLI ice-sheet model, Geosci. Model Dev., 7, 1377–1394, doi:10.5194/gmd-7-1377-2014, 2014.

Rommelaere, V. and Ritz, C.: A thermomechanical model of ice-shelf flow, Annals of Glaciology, 23, 13–20, 1996.

Rybak, O. and Huybrechts, P.: A comparison of Eulerian and Lagrangian methods for dating in numerical ice-sheet models, Annals of Glaciology, 37, 150–158, doi:10.3189/172756403781815393, 2003.

Schoof, C.: Ice sheet grounding line dynamics: Steady states, stability, and hysteresis, Journal of Geophysical Research (Earth Surface), 112, 2007.

Shapiro, N. M. and Ritzwoller, M. H.: Inferring surface heat flux distributions guided by a global seismic model: particular application to Antarctica, Earth and Planetary Science Letters, 223, 213–224, doi:10.1016/j.epsl.2004.04.011, 2004.

Stone, E. J., Lunt, D. J., Rutt, I. C., and Hanna, E.: Investigating the sensitivity of numerical model simulations of the modern state of the Greenland ice-sheet and its future response to climate change, The Cryosphere, 4, 397–417, doi:10.5194/tc-4-397-2010, 2010.

Tsai, V. C., Stewart, A. L., and Thompson, A. F.: Marine ice-sheet profiles and stability under Coulomb basal conditions, Journal of Glaciology, 61, 205–215, doi:10.3189/2015JoG14J221, 2015.

Waelbroeck, C., Labeyrie, L., Michel, E., Duplessy, J. C., McManus, J. F., Lambeck, K., Balbon, E., and Labracherie, M.: Sea-level and deep water temperature changes derived from benthic foraminifera isotopic records, Quaternary Science Reviews, 21, 295–305, doi:16/S0277-3791(01)00101-9, 2002.

Weertman, J.: On the Sliding of Glaciers, Journal of Glaciology, 3, 33–38, doi:10.3189/S0022143000024709, 1957.

Weertman, J.: Stability of the Junction of an Ice Sheet and an Ice Shelf, Journal of Glaciology, 13, 3–11, doi:10.3189/S0022143000023327, 1974.

Whitehouse, P. L., Bentley, M. J., and Le Brocq, A. M.: A deglacial model for Antarctica: geological constraints and glaciological modelling as a basis for a new model of Antarctic glacial isostatic adjustment, Quaternary Science Reviews, 32, 1–24, doi:10.1016/j.quascirev.2011.11.016, 2012.

Winkelmann, R., Martin, M. A., Haseloff, M., Albrecht, T., Bueler, E., Khroulev, C., and Levermann, A.: The Potsdam Parallel Ice Sheet Model (PISM-PIK) – Part 1: Model description, The Cryosphere, 5, 715–726, doi:10.5194/tc-5-715-2011, 2011.

Yan, Q., Zhang, Z., Gao, Y., Wang, H., and Johannessen, O. M.: Sensitivity of the modeled present-day Greenland Ice Sheet to climatic forcing and spin-up methods and its influence on future sea level projections, Journal of Geophysical Research: Earth Surface, 118, 2012JF002 709, doi:10.1002/jgrf.20156, 2013.

Geosci. Model Dev. Discuss., https://doi.org/10.5194/gmd-2018-105
Manuscript under review for journal Geosci. Model Dev.
Discussion started: 2 May 2018


Geoscientific Model Development Discussions
Open Access
EGU

**Table 1.** GRISLI model parameters used in this study.

| Variable | Identifier name | Value |
|---|---|---|
| Global constants | | |
| Gravitational acceleration | $g$ | $9.81\ m\ yr^{-1}$ |
| Water density, liquid | $\rho_w$ | $1000\ kg\ m^{-3}$ |
| Water density, ice | $\rho_i$ | $918\ kg\ m^{-3}$ |
| Water density, ocean | $\rho_o$ | $1028\ kg\ m^{-3}$ |
| Isostasy | | |
| Mantle density | $\rho_m$ | $3300\ kg\ m^{-3}$ |
| Relaxation time in isostasy | $\tau_m$ | $3000\ yr$ |
| Lithosphere flexural rigidity | $D_l$ | $9.87 \times 10^{24}\ N.m$ |
| Radius of relative stiffness | $R_l$ | $131910\ m$ |
| Radius of action of a unit mass | $R_{iso}$ | $400\ km$ |
| Hydrology | | |
| Thickness of the till layer | $h_{till}$ | $10\ m$ |
| Porosity of the till layer | $\phi_{till}$ | $0.5$ |
| River channel depth | $h_{river}$ | $10\ m$ |
| Deformation | | |
| Transition temperature of deformation, Glen | $T_3^{\text{trans}}$ | $-6.5\,^{\circ}\text{C}$ |
| Activation energy below transition, Glen | $Q_3^{\text{cold}}$ | $7.820 \times 10^4\,\text{J mol}^{-1}$ |
| Activation energy above transition, Glen | $Q_3^{\text{warm}}$ | $9.545 \times 10^4\,\text{J mol}^{-1}$ |
| Transition temperature of deformation, linear | $T_1^{\text{trans}}$ | $-10\,^{\circ}\text{C}$ |
| Activation energy below transition, linear | $Q_1^{\text{cold}}$ | $4.0 \times 10^4\,\text{J mol}^{-1}$ |
| Activation energy above transition, linear | $Q_1^{\text{warm}}$ | $6.0 \times 10^4\,\text{J mol}^{-1}$ |
| Temperature | | |
| Latent heat of ice fusion | $L_f$ | $335 \times 10^3\,\text{J kg}^{-1}$ |
| Ice thermal conductivity | $k_i$ | $1.04 \times 10^8\,\text{J m}^{-1}\text{K}^{-1}\text{yr}^{-1}$ |
| Mantle thermal conductivity | $k_b$ | $1.04 \times 10^8\,\text{J m}^{-1}\text{K}^{-1}\text{yr}^{-1}$ |

Geosci. Model Dev. Discuss., https://doi.org/10.5194/gmd-2018-105
Manuscript under review for journal Geosci. Model Dev.
Discussion started: 2 May 2018


Geoscientific Model Development Discussions
Open Access
EGU

**Table 2.** Selected parameters included in the LHS with their associated ranges.

| Parameter | Units | Minimum | Maximum |
|---|---|---|---|
| $E_{SIA}$ | – | 1. | 5. |
| $C_f$ | $yr\ m^{-1}$ | $0.5\ 10^{-3}$ | $5.\ 10^{-3}$ |
| $K_0$ | $m\ yr^{-1}$ | $20.10^{-6}$ | $200.10^{-6}$ |
| $b_{melt}$ | – | 0.75 | 1.25 |

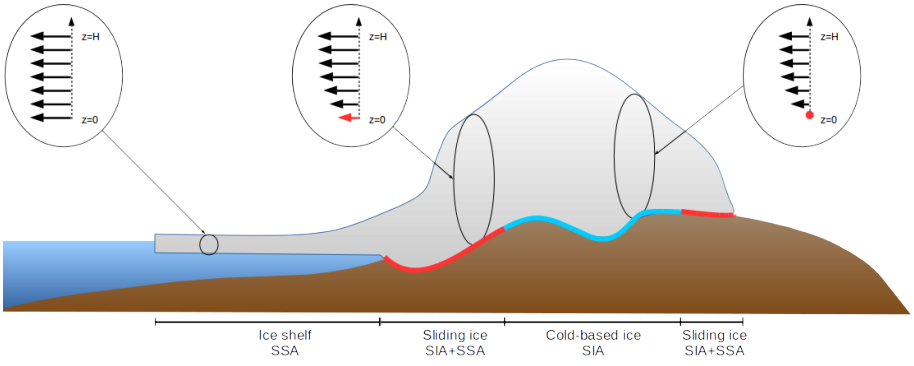


**Figure 1.** Schematic representation of the different types of flows in GRISLI and their associated velocity profiles. The red arrows stand for the sliding velocity which is non-zero for temperate-based grounded regions.

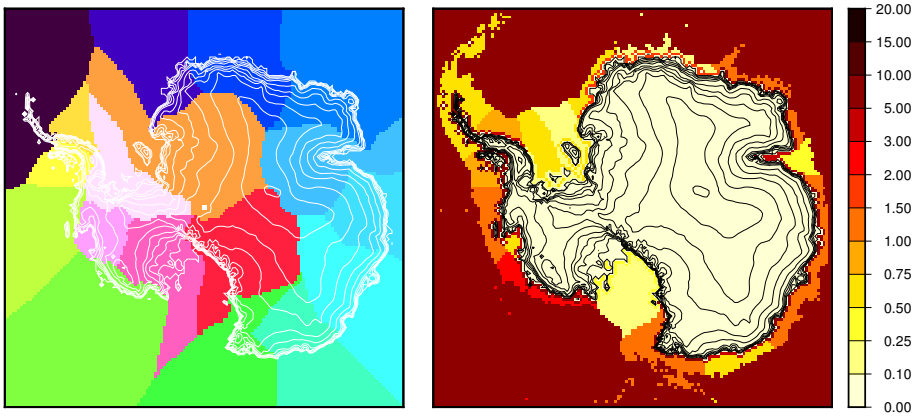


**Figure 2.** Antarctic ice shelves sectors (left) and associated prescribed present-day sub-shelf basal melting rates in $m\ yr^{-1}$ (right). The melting rates are different for the shelf and the associated grounding line.

Geosci. Model Dev. Discuss., https://doi.org/10.5194/gmd-2018-105
Manuscript under review for journal Geosci. Model Dev.
Discussion started: 2 May 2018


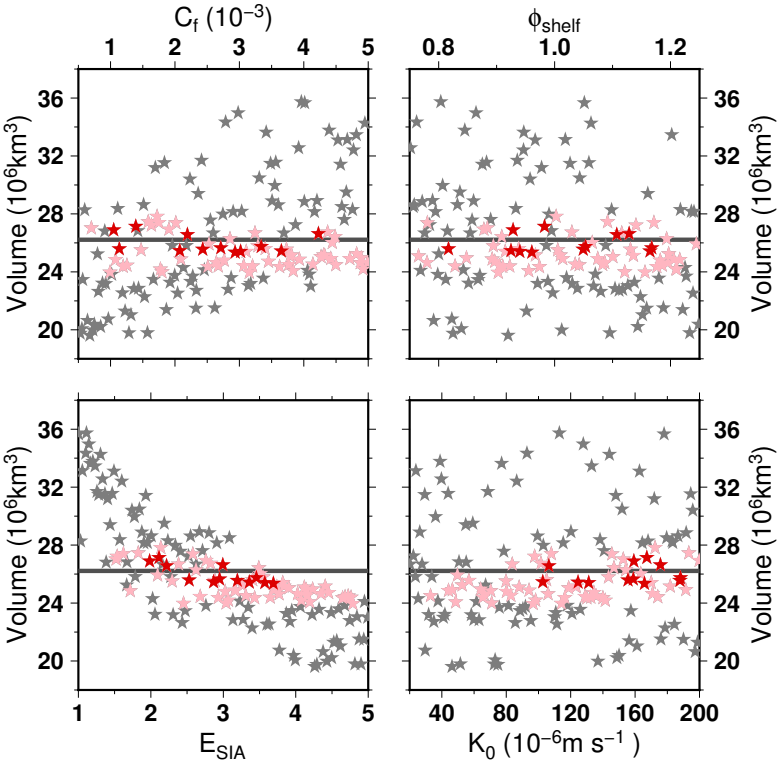


**Figure 3.** Simulated total ice volume for each ensemble members as a function of parameter values when using the Schoof (2007) formulation of the flux at the grounding line (AN40S). The thick horizontal line stands for the observations (Fretwell et al., 2013). Colored stars correspond to the ensemble members that have a RMSE lower than 350 m. The dark red stars represent the 12 ensemble members that yield the lowest RMSE.

Geosci. Model Dev. Discuss., https://doi.org/10.5194/gmd-2018-105
Manuscript under review for journal Geosci. Model Dev.
Discussion started: 2 May 2018


Geoscientific Model Development Discussions

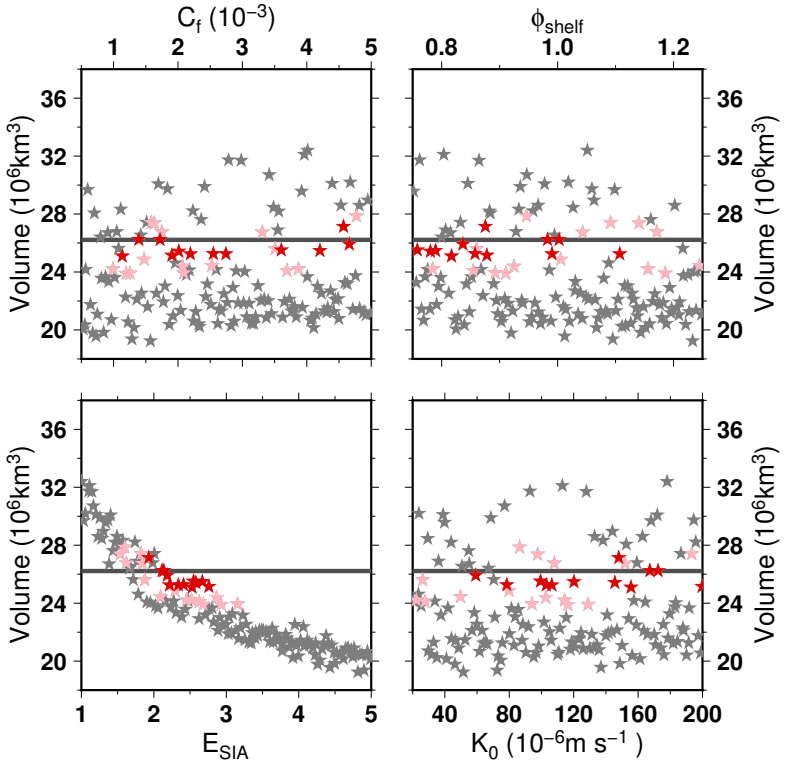


**Figure 4.** Same as Fig. 3 but with the Tsai et al. (2015) formulation of the flux at the grounding line (AN40T).

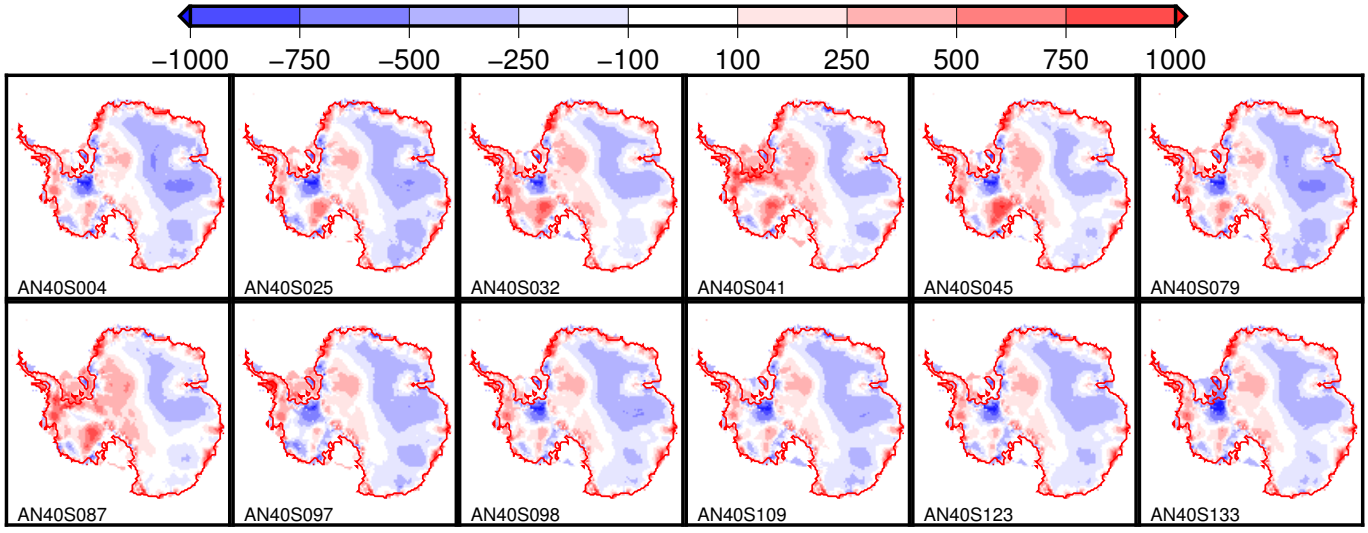


**Figure 5.** Ice thickness difference with the observations (simulated minus observed) from the 12 ensemble members showing the lowest RMSE when using the Schoof (2007) formulation of the flux at the grounding line (AN40S).

Geosci. Model Dev. Discuss., https://doi.org/10.5194/gmd-2018-105
Manuscript under review for journal Geosci. Model Dev.
Discussion started: 2 May 2018


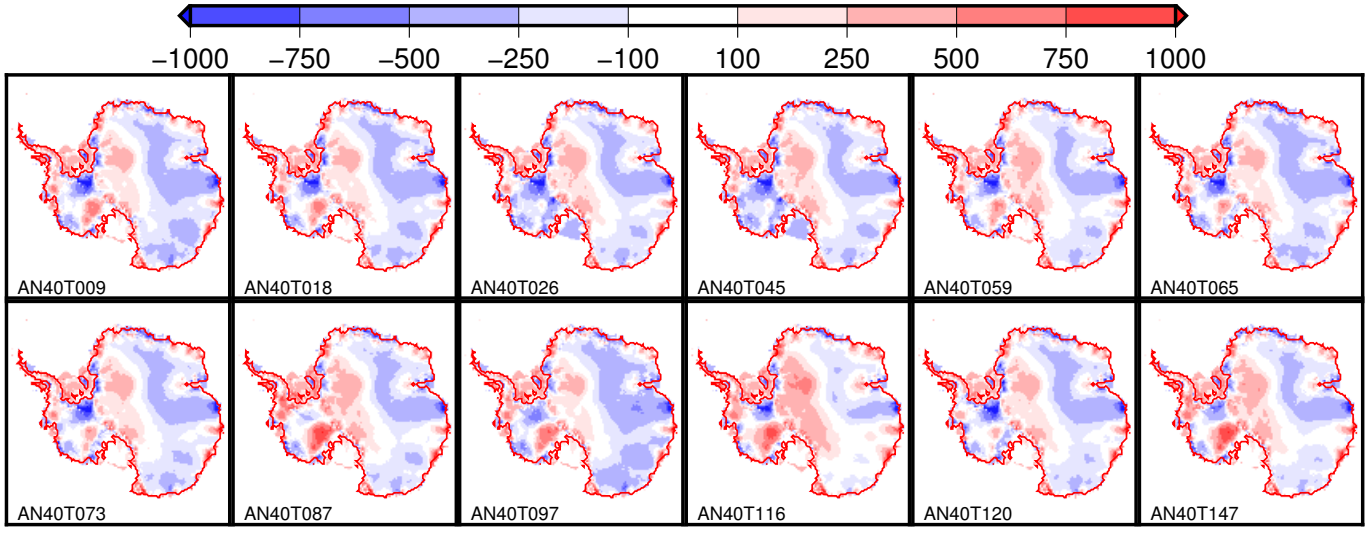


**Figure 6.** Same as Fig. 5 but with the Tsai et al. (2015) formulation of the flux at the grounding line (AN40T).

Geosci. Model Dev. Discuss., https://doi.org/10.5194/gmd-2018-105
Manuscript under review for journal Geosci. Model Dev.
Discussion started: 2 May 2018


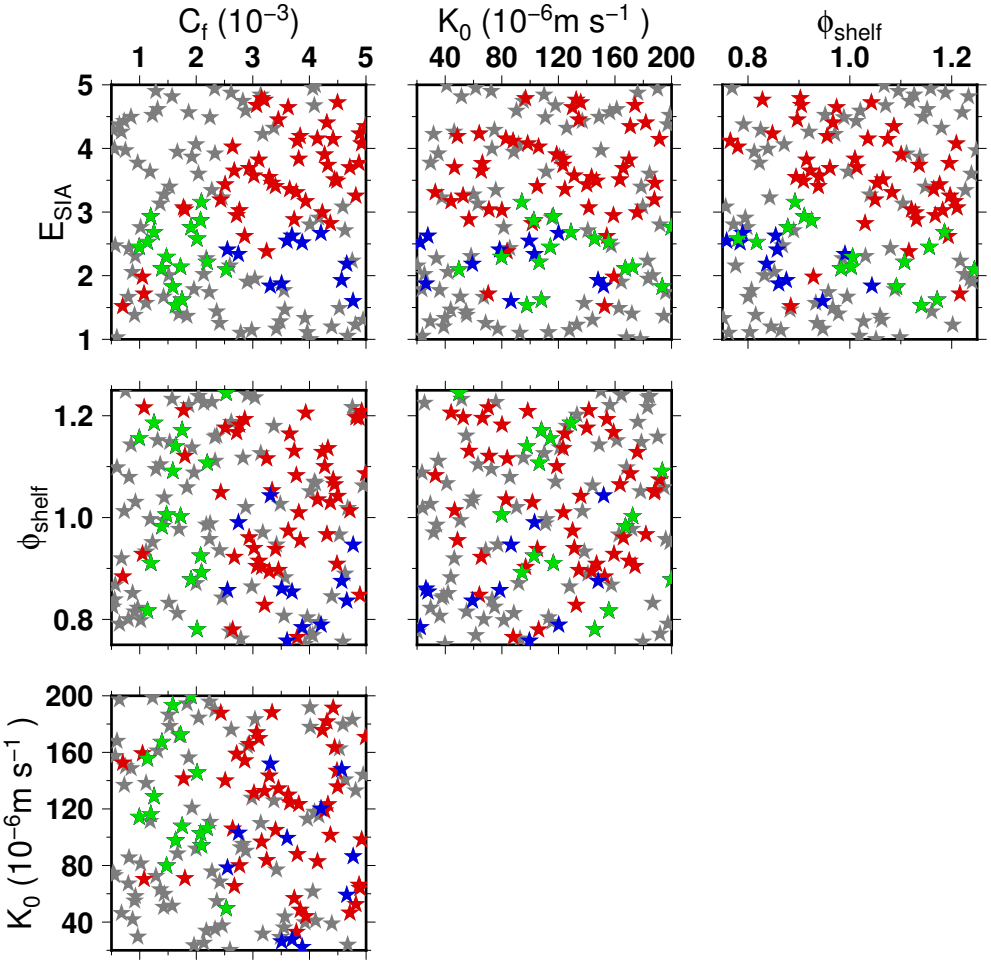


**Figure 7.** Distribution of the 150 model parameter values. The ensemble members that present a RMSE lower than 350 m are colored: Schoof (2007) formulation (red), Tsai et al. (2015) (blue) and both (green).

Geosci. Model Dev. Discuss., https://doi.org/10.5194/gmd-2018-105
Manuscript under review for journal Geosci. Model Dev.
Discussion started: 2 May 2018


Geoscientific Model Development Discussions

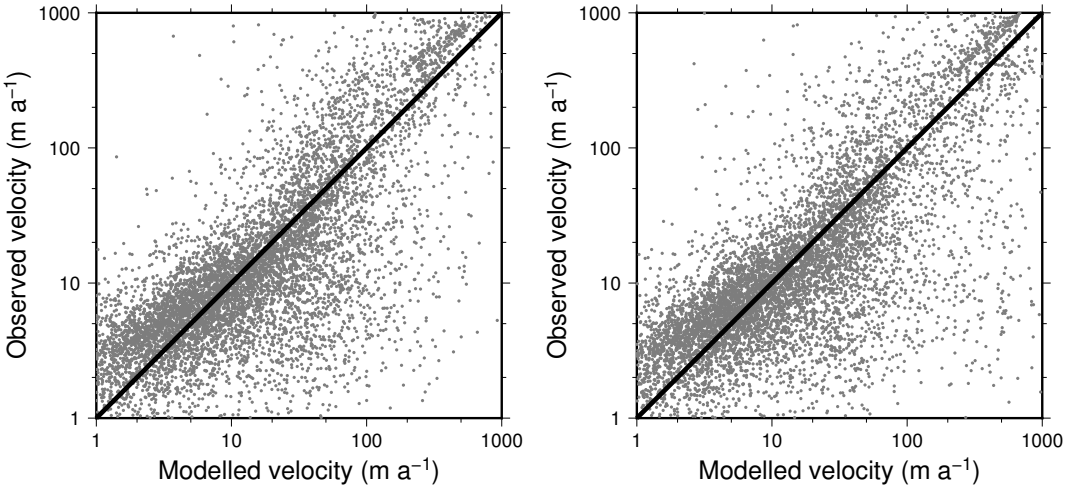


**Figure 8.** Observed velocity (Mouginot et al., 2017) against modelled velocity on the 40 km grid. Only the best ensemble members with the lowest RMSE is shown here for Schoof (2007) (AN40S109, left) and Tsai et al. (2015) (AN40T120, right). AN40S109 has $E_{SIA} = 3.36$, $C_f = 3.7\ 10^{-3}\ yr\ m^{-1}$, $K_0 = 125\ 10^{-6}\ m\ yr^{-1}$ and $\phi_{shelf} = 1.16$ and AN40T120 has $E_{SIA} = 2.67$, $C_f = 4.2\ 10^{-3}\ yr\ m^{-1}$, $K_0 = 120\ 10^{-6}\ m\ yr^{-1}$ and $\phi_{shelf} = 0.79$.

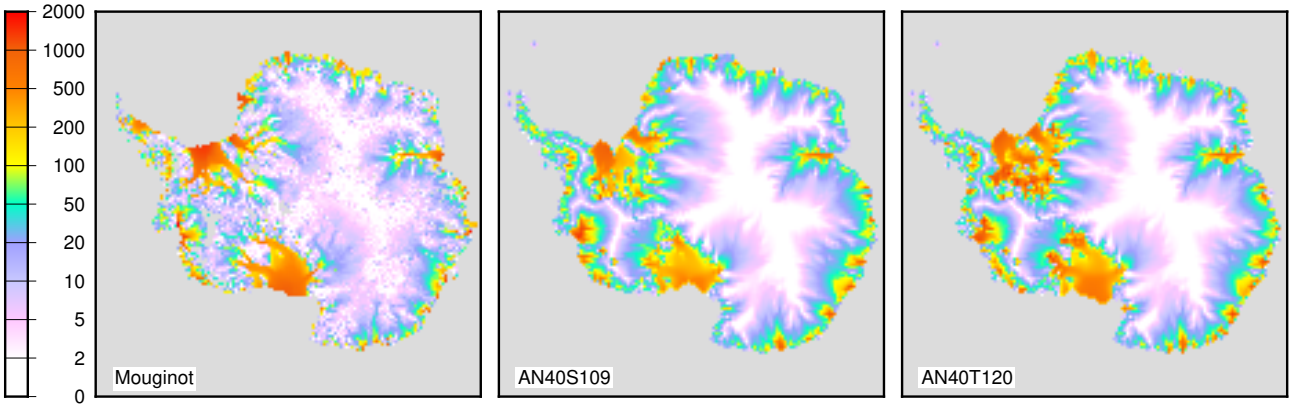


**Figure 9.** Map of observed (Mouginot et al., 2017) and simulated velocities in $m\ yr^{-1}$ for the ensemble members with the lowest RMSE using Schoof (2007) (AN40S109) and Tsai et al. (2015) (AN40T120).

Geosci. Model Dev. Discuss., https://doi.org/10.5194/gmd-2018-105
Manuscript under review for journal Geosci. Model Dev.
Discussion started: 2 May 2018


Geoscientific Model Development Discussions
Open Access
EGU

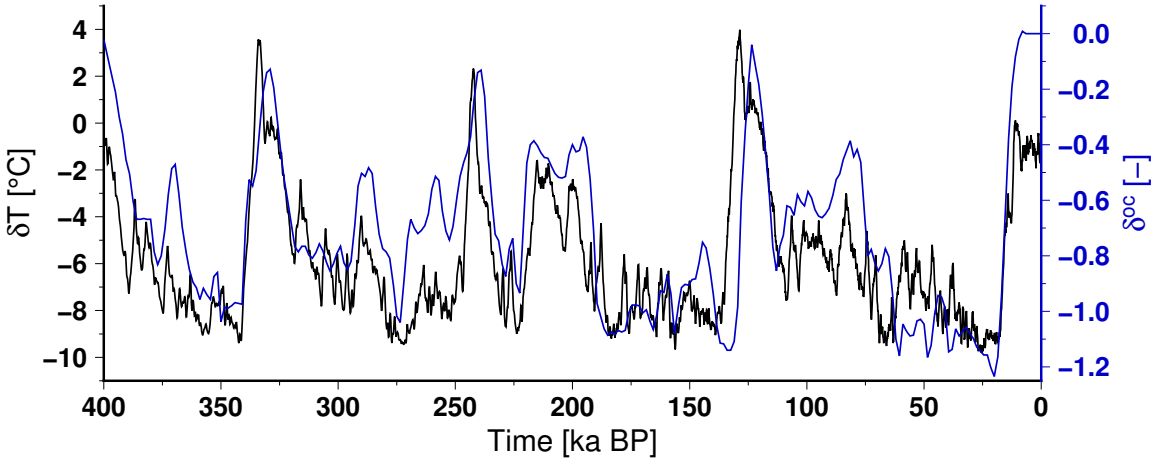


**Figure 10.** Climatic perturbation used in the 400 kyr glacial-interglacial simulations for the near-surface air temperature, $\delta T = \left(1/\alpha^{i}\right)\delta D$, and for the sub-shelf basal melting rate modificator, $\delta^{oc} = \alpha^{oc}\,\Delta T_{NA}/T_{NA0}$.

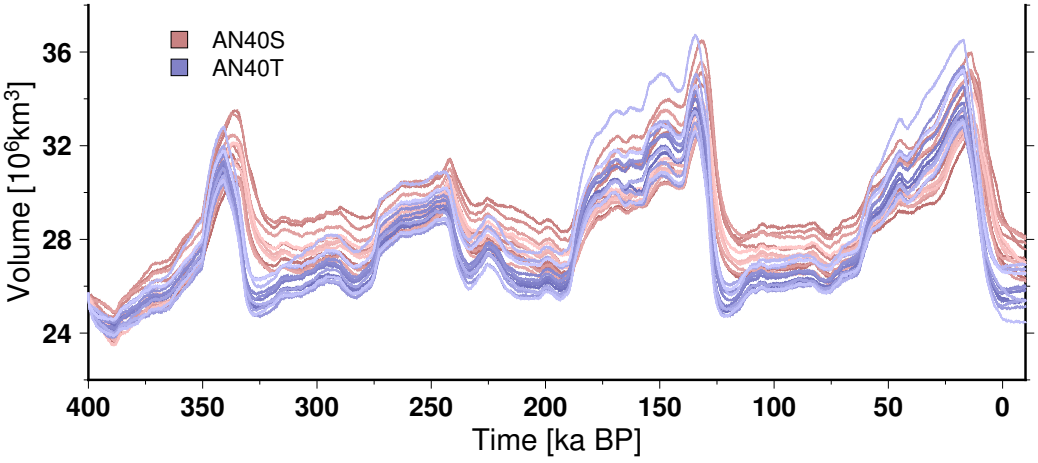


**Figure 11.** Simulated total ice sheet volume evolution over the last 400 kyr for the twelve ensemble members showing the lowest RMSE in Sec. 3 when using the flux at the grounding line computed from Schoof (2007) (AN40S, shade of reds) and Tsai et al. (2015) (AN40T, shade of blues). The glacial to interglacial difference in ice volume for the last termination corresponds to about -10 to -20 m of global sea level rise equivalent depending on the simulations.

Geosci. Model Dev. Discuss., https://doi.org/10.5194/gmd-2018-105
Manuscript under review for journal Geosci. Model Dev.
Discussion started: 2 May 2018


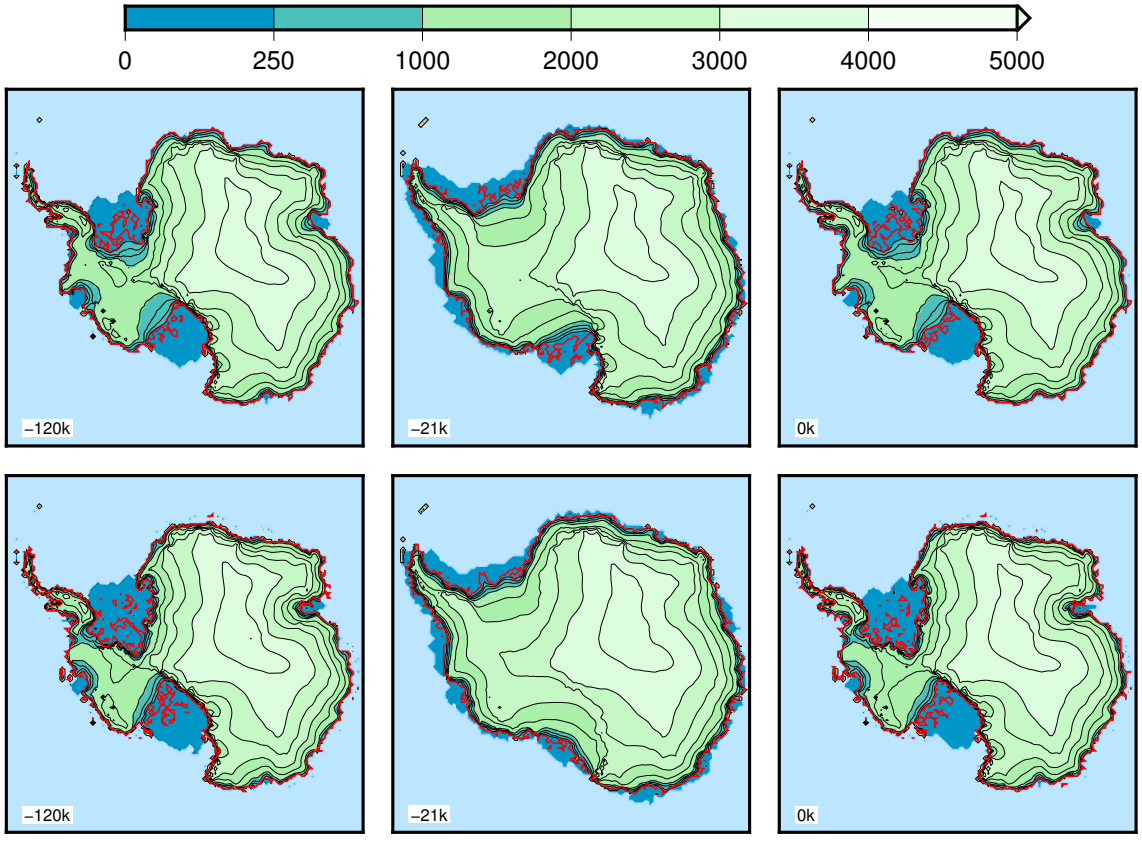


**Figure 12.** Simulated surface elevation at selected snapshots for the two ensemble members that produce the minimal RMSE at 0 kaBP in the transient simulations (AN40S097, top, and AN40T059, bottom). The ice volume contributing to sea level change from present is -10.8 m (resp. -19.9 m) at 21 kaBP for AN40S0097 (resp. AN40T059), whilst it is negligible (less than 6 centimetres) at 120 kaBP. The grounding line is materialised by the thick red line.

Geosci. Model Dev. Discuss., https://doi.org/10.5194/gmd-2018-105
Manuscript under review for journal Geosci. Model Dev.
Discussion started: 2 May 2018


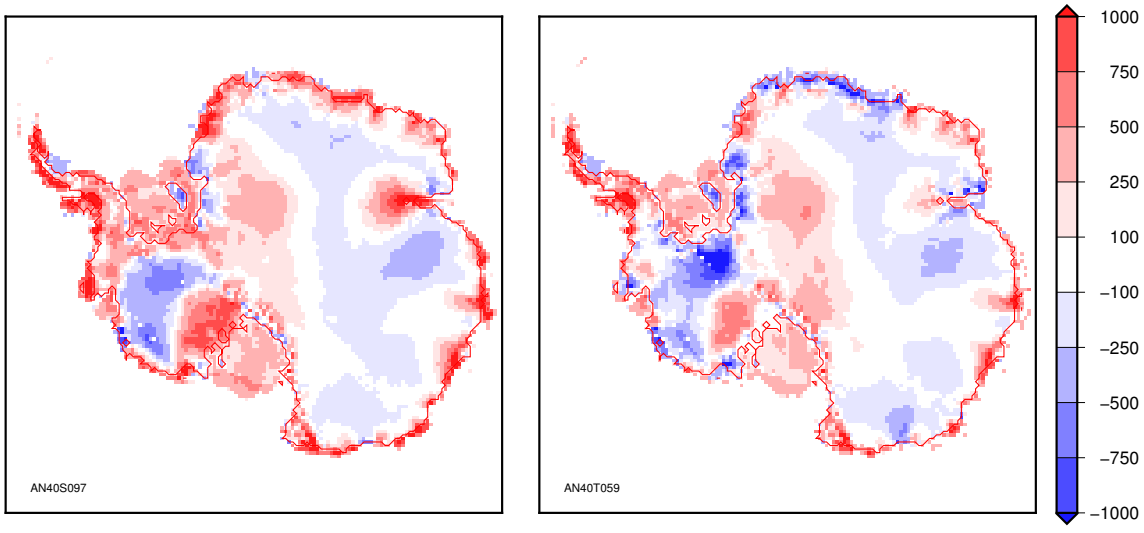


**Figure 13.** Ice thickness difference with the observations (simulated minus observed) at 0 ka BP for the two ensemble members that produce the minimal RMSE at 0 kaBP in the transient simulations (AN40S097, left, and AN40T059, bottom). The RMSE is 360 m (respectively 314 m) for AN40S097 (resp. AN40T059).